JAERI-M
9071

"STUDIES ON IRRADIATION BEHAVIORS OF COATED PARTICLE FUELS"

August 1980

Kousaku FUKUDA, Kazumi IWAMOTO and
Katsuichi IKAWA

日本原子力研究所
Japan Atomic Energy Research Institute

この報告書は，日本原子力研究所がJAERI-Mレポートとして，不定期に刊行している研究報告書です．入手，複製などのお問合わせは，日本原子力研究所技術情報部（茨城県那珂郡東海村）あて，お申しこしください．

JAERI-M reports, issued irregularly, describe the results of research works carried out in JAERI. Inquiries about the availability of reports and their reproduction should be addressed to Division of Technical Information, Japan Atomic Energy Research Institute, Tokai-mura, Naka-gun, Ibaraki-ken, Japan.

JAERI-M 9071

"Studies on Irradiation behaviors of Coated Particle Fuels"

Kousaku FUKUDA, Kazumi IWAMOTO and Katsuichi IKAWA

Division of Nuclear Fuel Research,
Tokai Research Establishment, JAERI

(Received August 13, 1980)

This report is concerned with the principal results of the irradiation experiments of TRISO coated particle fuels performed at JAERI. Followings on the irradiation experiments are described.

1) Irradiation tests of the coated particle fuels performed at JAERI.
2) Summary of the irradiation capsules and OGL-1 fuel specimens, and measurements of temperatures, burnup and neutron fluence.
3) Some results on kernels, anisotropy of the PyC layers and crushing strength of the irradiated particles.
4) Diffusion coefficients of ^{133}Xe, ^{140}Ba, ^{89}Sr, ^{141}Ce and ^{103}Ru in the slightly irradiated SiC.
5) Release behaviors of the gaseous fission products from the particle fuels in the gas swept capsules and OGL-1.
6) Concentration distributions of ^{137}Cs and ^{90}Sr in the irradiated TRISO particles.

Keywords: HTGR Fuels, TRISO Coated Particles, Irradiation Behaviors, Capsules, OGL-1, Fuel Specimen, Kernel, P_yC Layer, Anisotropy Factor, SiC Layer, Diffusion Coefficients, Fission Products

被覆燃料粒子の照射挙動の研究

日本原子力研究所東海研究所燃料工学部
福田　幸朔・岩本多実・井川勝市

（１９８０年８月１３日受理）

本報告は，日本原子力研究所におけるＴＲＩＳＯ型被覆燃料粒子の照射及びその照射結果に関するものである。ここでは，これらの照射試験について次のことが述べられる。

1） 日本原子力研究所における高温ガス炉燃料の照射実績
2） 照射キャプセル及びOGL－1装置の概要，及び温度，燃焼度，中性子照射量の測定
3） 照射された被覆粒子の燃料核，ＰｙC層の異方性及び破壊強度に関する結果
4） 低照射したSiC中の ^{133}Xe，^{140}Ba，^{89}Sr，^{141}Ce 及び ^{103}Ru の拡散係数
5） ガス・スイープキャプセル及びOGL－1装荷粒子からのＦＰガス放出挙動
6） 照射したＴＲＩＳＯ被覆粒子中の ^{137}Cs，及び ^{90}Sr の濃度分布

Contents

目　　次

List of Tables

List of Figures

"Studies on Irradiation behaviors of Coated Particle Fuels"

1. Introduction

Project for development of an experimental HTGR in Japan was started at JAERI in 1970 in order to utilize the process heat for the multi purposes. Temperature of the outlet gas is designed to be 1000°C and so the HTGR is called as the experimental Very High Temperature Reactor(VHTR). The VHTR is a helium-cooled graphite moderated reactor with the thermal out-put of 50 MW. The fuel specification for the VHTR by First Conceptional Design is listed in Table 1. It is characteristic that the enrichment of uranium-235 desiged for the driver fuels of the VHTR is low such as 2, 4 and 6 %. Therefore, the maximum burnup of the fuels is estimated to be 3 %FIMA for the effective full power days,360 days, and also the maximum fast neutron fluence($E > 0.18$MeV), 1.5×10^{21} n/cm^2[1]. Maximum fuel temperature is, however, relatively high, 1350°C, and 0.01 % of the fuels in the reactor core is estimated to be over 1500°C for a certain period of the fuel life[2].

The irradiation experiments of the coated particle LEU fuels refered to First Conceptional Design have been made in JMTR and JRR-2 so as to meet the above irradiation conditions of the driver fuels.

In JMTR, the first irradiation of the coated particles by the closed capsule was performed in 1970 and since then, 10 closed capsules for the coated fuel partilces and the fuel compacts were irradiated. The gas-swept capsule at JAERI was firstly irradiated in 1977

and at present, the two are under irradiation. Also in 1977, a high-pressure helium-gas in-pile loop, OGL-1, was installed to JMTR and the irradiation experiments of the particle fuels by the loop were started. On the other hand, the irradiation experiments in JRR-2 are principally intended to examine the amoeba effect in the coated particles and to measure the thermal conductivities of the fuel compacts under irradiation.

Due to the partial amendment of the law for the nuclear fuel transportation, it was impossible to transport the irradiated capsules from JMTR to Tokai hot laboratory for about three years from Jan. 1977 to Mar. 1980 when the new cask was available. Therefore, PIE schedule at JAERI was delayed greatly.

In this report, the principal results with regard to LEU fuel performance assessment obtained in the irradiation experiments at JAERI are described.

2. Irradiation

2.1 Irradiation performance

Irradiation of the coated particle fuels for the VHTR performed in JMTR is shown as a relation between fast neutron fluence and burn-up in Fig. 1. As mentioned above, maximum burnup and fast neutron fluence designed for the VHTR are relatively low and therefore, these irradiation conditions attained in our experiments are not so severe; for instance, maximum burnup was 4 %FIMA(73F-13A) and maximum fast neutron fluence, 2.3×10^{21} n/cm^2 (E>0.18 MeV).

In OGL-1 experiments, the fourth fuel is under irradiation at present. Burnup of this fuel will attain to the maximum (about 2 %FIMA) among the former OGL-1 fuels. Fast neutron fluence of this fuel is, however, very low, usually less than 1×10^{20} n/cm^2 (E > 0.18 MeV).

2.2 Summary of irradiation capsules

Irradiation capsules for JMTR consist of one or three inner capsules, each of which is equipped with thermocouples and a small tube for temperature control. Typical JMTR irradiation capsules are shown in Fig. 2; the upper capsule consisting of three inner capsules is used generally to irradiate the small size of the fuel compacts(24 mm in outer diameter) or the loose coated fuel particles. Fuel temperature at each inner capsule is individually controlled by a dgree of vacuum at a space between the walls within the inner capsule. Structure of the gas swept capsule is principally the same as this capsule, but the swept capsule is equipped with a tube for the seep gas. The capsule shown below in Fig. 2 is used

for irradiation of the fuel compacts encased in a long graphite sleeve. It is possible to make temperatures of the compacts flat along an axial direction from the bottom to the top in the capsule by adjusting the gap between the sleeve for the compacts and the inner capsule.

Irradiation experiments of the coated particle fuels are also performed in OGL-1 as mentioned. Main specifications of OGL-1 are listed in Table 2 and one of the fuel specimens for OGL-1 is shown in Fig. 3(4th fuel). The fuel specimen consists of the graphite block and the fuel pins inserted in the block. We have two types of the fuel specimens, one of which loads one fuel pin and the other, three pins as shown in Fig. 3. 20 fuel compacts are encased into one fuel pin. Temperatures of the fuel compacts and the block are measured by the thermocouples and analysed by the computer. Gaseous fission products released from the compacts and carried by the circulating helium gas are measured at the sampling station attached in front of the purification system.

Irradiation capsules for the amoeba effects in JRR-2, contain, generally, 60 - 90 graphite disks in which the coated particles are embeded. At a central hole of stacked graphite disks, the loose coated particles are loaded in order to attain a temperature gradient through the disks. The gradient is about 25°C/mm at 1600°C.

2.3 Measurements of temperature, burnup and fast neutron fluence

Measurements of the fuel temperature in a capsule are made by W/Re thermocouples inserted into a central hole of the compacts stacked in a capsule(Fig. 2) or into the graphite holders for the coated particles. In the JMTR capsules, the thermocouples are usually equipped at an upper-, a middle- and a bottom inner capsule, or at three positions along an axial direction in a capsule if the capsule includes only a long inner capsule. In the case of OGL-1, the temperature of the fuel compacts is calculated by the computer code"STPDSP2"[3] based on the measured temperatures in the cycling gas, the graphite block and at a central position of the stacked compacts in each fuel pin (Fig. 3). Fig. 4 shows a typical example of the fuel temperature obtained in the first OGL-1 experiment.

Burnup of the fuels is usually obtained by the measurements as follows: Five coated particles from a sample(a compact or loose coated particles) were, at first, counted individually to measure ^{137}Cs inventory by a γ-ray spectrometer and then, a content of uranium at each particle was analyzed by the electrochemical method. Burnup of the other samples in the capsule was obtained by an extrapolation of the measured values in the capsule geometry as shown in Fig. 5, or by the neutron distribution along an axial direction of the capsule.

Fast neutron fluence is measured by the reaction $^{54}Fe(n,p)^{54}Mn$ (half life, 313 days) of Fe monitor wires attached to a capsule. Comparison of fast neutron fluence distributions by measurements and calcualtion is shown in Fig. 6 as a typical example. In this case, it is seen that the measured fast neutron fluence is somewhat higher than the calcualted one at a central position, but a difference between measurements and calculation is hardly noticed at the other positions.

3. Results

3.1 Irradiation results of coated fuel particles

3.1.1 Irradiation behaviors of kernels

Irradiation behaviors of the kernels are investigated by both ceramography and X-ray micraradiography in PIE. Typical features observed in the kernels of irradiated TRISO particles are

(1) kernel shrinkage,

(2) kernel migration (the amoeba effect)

(3) kernel viscous flow.

As shown in Fig. 7, it was observed that the low-density kernels (90 %T.D.) of the coated particles irradiated upto about 2.7 %FIMA at 1000°C shrinked more remarkably than the middle-density kernels (95 %T.D.). The kernels of low density shrinked mostly interacting with the buffer layer which peeled from the inner PyC layer(Fig. 7).

Kernel migration is often observed in the loose coated particles and the compacts irradiated in JMTR. Fig. 8 shows the typical example of the kernel migration phenomena (amoeba effect) observed in the particles which were irradiated in Capsule 73F-12A.

According to the irradiation experiments in JRR-2, the amoeba effect in the coated particles irradiated upto 1300 hrs under temperature gradients, 18°C/mm and 20°C/mm, at 1070° and 1250°C, respectively, was not observed. However, in irradiation at 1600°C, the effect was observed in spite of the lower temperature gradient, 10°C/mm, than the formers. Kernel migration coefficients will be obtained in near future.

When there is a wide crack in the buffer layer, it is seen that the kernel material (UO_2) moves into the crack like a viscous flow as shwon in Fig. 9. It seemed that the phenomena is not

related to the amoeba effect and irradiation temperature; for instance, the coated particles,71FC5, in Fig. 9 were irradiated at 1190-1070°C which is very low compared to the melting point of UO_2, 2760°C[4], and also the amoeba effect in these particles was not observed. The cause of this phenomena is not clear at present.

3.1.2 Precipitation of solid fission products

In the irradiated coated particles, the white precipitates were observed. They were not examined by a XMA, but seemed to be an agglomerates of solid fission products. The precipitates are classified into two groups, Ba free precipitates and Ba contained ones[5]. As shown in Fig. 10, diameter of these precipitates might be constant (1 - 2.5 μm) independently on burnup of the kernels, but number of the precipitate seen in a unit area would increase with burnup. Also the precipitates appeared always at the grain boundaries,and some of them were seen particularly at the nodal points of the boundaries.

X-ray microradiography of relatively highly-irradiated particles revealed some dark spots in the buffer layer particularly near the interface between the buffer and inner PyC layers as shown in Fig. 11. Since these spots appeared only in highly irradiated particles(>2 %FIMA), we believe that these are the segregation of the solid fission products. Among the fission products, Cs and Ag are volatile and do not dissolve in the UO_2 matrix[5]; these nuclides show the similer diffusion behaviors in the UO_2[6]. However, Ag passes through the coating layer, while Cs does not do so[7]. Cs is retained more firmly in the high density PyC layer than e.g. Sr under irradiation[5]. Therefore, the dark spots would be the precipitates of the volatile fission products such as Cs which migrate through the buffer layer to one

direction due to slight temperature gradient under irradiation.

3.1.3 OPTAF of PyC layers on irradiated TRISO coated particles

OPTAF of LTI-PyC layers(outermost PyC and inner PyC) on the irradiated TRISO coated particles was measured. Irradiation temperatures of these particles were in the range between 1000° and 1740°C, burnup , between 0.1 and 2.5 %FIMA, and fast neutron fluence ($E > 0.18$ MeV), between 6×10^{18} and 1.4×10^{21} n/cm^2. Variation of OPTAF of the PyC layers with fast neutron fluence is shown in Fig. 12. It is seen in the figure that OPTAF increases with fast neutron fluence. OPTAF of the outer PyC would be somewhat higher than that of the inner PyC. Temperature dependence of OPTAF is also seen in the figure; at low fluence of fast neutron, temperature dependence of OPTAF is not so remarkable but at the high fluence, 1×10^{21} n/cm^2, the temperature dependence becomes evident.

Furthermore, distributions of OPTAF through the PyC coating layers were measured. Results obtained from the particle irradiated at 1300°C upto 1.4×10^{21} n/cm^2 ($E > 0.18$ MeV) of fast neutron fluence, are shown in Fig. 13. In the figure, it is seen that OPTAF values in both the outer and inner PyC layers increase with approching the SiC layer. This would imply that the PyC layers were holded by the SiC layer against their dimensional change and therefore, stress was introduced so as to increase OPTAF values in the PyC layers.

3.1.4 Residual stress in outermost PyC layer due to anisotropy

In Capsule 72F-6A and 72F-7A of JMTR, we irradiated several kinds of TRISO coated particles, of which the outermost PyC layers have different anisotropy(from 1.03 to 1.26 in BAF). These PyC

layers were derived from either propane or propene. In ceramography of PIE, the outermost PyC layer possessing high value of BAF, was cracked radially, as shown in Fig. 14. Comparing the surface inspection of cracked and uncracked coated particles, it is evident that these cracks are brought about during polishing of ceramography. Hence, it is considered that the outermost PyC layer with high value of BAF become to possess high residual stress by irradiation and the stress causes the cracks during polishing. According to Bokros et al[8], large stress is introduced at crystal boundaries of PyC due to irradiation-induced dimensional change that are highly anisotropy.

In Fig. 15, a relation between fast neutron fluence, BAF and the residual stress judged by crack formation is indicated. In the figure, it is seen that there is a threshold value of BAF to endure the crack formation during polishing, that is 1.04. However, under low fast neutron fluence below 0.25×10^{21} n/cm^2 ($E > 0.18$ MeV), the PyC layers are free from the cracks despite the high value of BAF. With regard to BAF, Harmon et al[9] found that outermost PyC layer of TRISO particles with anisotropy values of ≥ 1.05(BAF unit) exhibited the best performance for irradiation. In the present case, although fast neutron fluence is very small compared to the former[9], the BAF value is desirable less than 1.04 in the view point of the residual stress in the outer PyC layer.

3.1.5 Crushing strength of unirradiated- and irradiated TRISO coated particles

To examine the state of deterioration of the coated particles

by irradiation , crushing strength of TRISO coated particles was measured. Fig. 16 shows a typical example of a load-deflection curve for an irradiated TRISO particle. In the figure, the first load with deflection was brought about from the layers and the latter, from the kernel. For the measurements of the mean strength of the irradiated particles, about 25 particles were crushed. In Fig. 17, Weibull plots of the failure loads of unirradiated and irradiated TRISO particles are shown. It is seen in the figure that the crushing load decreases, on the whole, with increase of irradiation conditions, and Weibull modulus of irradiated particles becomes smaller compared to that of unirradiated ones.

Relation between mean loads of the layers and the kernels, and irradiation conditions are shown in Fig. 18. In the figure, it is seen that the crushing loads of the layers decrease in the range between 50 % and 70 % under fast neutron fluence of 1.0×10^{21} n/cm^2, and on the other hand, that of the kernels, between 40 % and 60 % upto 2.2 %FIMA of burnup. The former deterioration would be due to damage by fast neutron and high temperature, and the latter, due to the formation of the fission gas voids at the grain boundaries as shown in Fig. 10.

3.2 Fission product migration

3.2.1 Diffusion coefficients of fission products in SiC

Since the TRISO coated particle fuels are used at relatively high temperature(max. nominal temperature 1350°C) in the VHTR, it is important to obtain the diffusion coefficients of the fission products in SiC. In our experiments to obtain the coefficients in SiC, the samples were not heavily irradiated but slightly in JRR-2.

(1) ^{133}Xe diffusion coefficients in SiC

Two different SiC samples were used to measure ^{133}Xe diffusion coefficients in SiC; one was the powdered pyrolytic SiC which was immersed in uranylnitrate solution and then dried, and the other was SiC coated particles without high-density outermost PyC layer. These samples were irradiated in JRR-2 for about 20 min to produce the fission products in the samples; particularly in the case of the powdered SiC, the fission products were recoiled into the powder. After slight irradiation, the powdered SiC samples were heated in two different manners as

1) stepwise from 1073° to 1657°C,

2) isothermally between 1465° and 1753°C,

and the fractional releases of ^{133}Xe were measured. The SiC coated particles were, on the other hand, isothermally heated between 1650° and 1850°C, and the releases were measured.

In the case of ^{133}Xe releases from the powdered SiC, the following equations were applied to obtain ^{133}Xe diffusion coefficients[10].

$$F(t) = 1 - \frac{24}{\nu^2(12-\nu^2)} \sum_{n=1}^{\infty} \left\{ \frac{\nu(2+\nu)}{(n\pi)^2} - \frac{2\sin(n\pi\nu)}{(n\pi)^3} - \frac{2[1-\cos(n\pi\nu)]}{(n\pi)^4} \right\} \times \exp(-Dtn^2\pi^2/a^2) \quad , \quad (1)$$

or when the fractional release is less than 0.3,

$$F(t) = \frac{24(\nu+2)}{\nu(12-\nu^2)}\left(\frac{Dt}{\pi a^2}\right)^{0.5}, \qquad (2)$$

where F is the fractional release, ν a ratio of the recoil range to the sphere redius a, D the diffusion coefficient and t the time. Analysis of the fractional releases from the sample heated stepwise were made as follows; as shown in Fig. 19, the releases were plotted against $\sqrt{t}$, where t was a duration from begining of heating at a constant temperature. From the gradients of the fractional releases, the diffusion coefficients were obtained by Eq. (2).

The diffusion coefficients in this manner, however, might include an error, particularly with increase of heating temperaure because of decrease of ^{133}Xe concentration at the surface region of the SiC powder. Comparing an initial concentration of ^{133}Xe inside the powder at 1657°C, the maximum temperature in this heating, and a constantly distributed concentration, it can be estimated that the fractional release from the former concentration at 1657°C is only 1.1 times less than the release from the latter concentration at that temperature. This leads to the consideration that the diffusion coefficients by stepwise heating are about 83 % of the coefficients by isothermal heating at 1657°C , and also the error of the coefficients at the lower temperatures than 1657°C is surely less than that at 1657°C.

The results of the fractional releases by isothermal heating between 1465° and 1753°C are shown in Fig. 20. The diffusion coefficients were obtained from the gradients of the releases at 1465° and 1600°C as well as the former method,and the release at 1750°C was analyzed by Eq. (1) so as to fit the calculated farctio-

nal release to the experimental one with a proper diffusion coefficients.

Heating of SiC coated particles slightly irradiated in JRR-2 was made isothermally between 1650° and 1850°C. Fig. 21 shows the results of ^{133}Xe fractional releases. For the releases, Baurmann's model[11] was applied to obtain the diffusion coefficients.

Arrhenius plots of ^{133}Xe diffusion coefficients in SiC obtained hereupon are given in Fig. 22, where the self diffusion coefficients of Si and C[12], and the boundary diffusion coefficients[13] are included. In the figure, following two diffusion mechanisms can be distinguished:

(a) Above 1400°C, Arrhenius equations of the diffusion coefficients are expressed as

$D = 3.7 \times 10^{5} \exp(-657 \times 10^{3}/RT)$ cm^2/sec .... SiC powder,

$D = 1.7 \times 10^{4} \exp(-624 \times 10^{3}/RT)$ cm^2/sec .... SiC coated particles,

where R is a gas constant (=8.314 J/K mol.) and T the absolute temperature (°K). Both of these diffusion coefficients fairly agree together despite the different crystallite size (the former is 1.8×10^{-8} m and the latter 10^{-5} m), and these high activation energies are almost the same as that of the carbon self diffusion coefficients (586×10^{3} J/mol.)[12] as shown in Fig. 22. Furthermore, an extraporation of these Xe diffusion coefficients to higher temperature agrees with Si diffusion coefficient. Therefore, it is considered that Xe diffusion in SiC above 1400°C occures in the vacancy mechanism, supposedly via Si vacancies or Si-C divacancies.

(b) Arrhenius equation below 1400°C is expressed as

$D = 8.6 \times 10^{-6} \exp(-327 \times 10^3/RT)$ $cm^2/sec.$

This activation energy fairly agrees with that of boundary self diffusion-coefficients, 306×10^3 J/mol.[13]. Therefore, it is concluded that Xe diffusion below 1400°C is probably made in the boundary mechanism.

(2) Diffusion coefficients of solid fission products in SiC

The diffusion coefficients of solid fission products such as ^{89}Sr, ^{140}Ba, ^{103}Ru and ^{141}Ce were obtained by measuring the concentration distributions of the fission products through the SiC layer and also measuring the fractional releases under isothermal heating between 1650° and 1850°C.

^{89}Sr and ^{103}Ru concentration distributions were shown in Figs. 23 and 24 as the typical results. The calculated distributions by Baurmann model[11] were fitted to measured ones and the diffusion coefficients together with the evaporation coefficients and the partition coefficients between SiC and inner PyC layers, were obtained. Then, the fractional releases calculated with the above parameters were compared with the experimental results. In the case of ^{140}Ba and ^{89}Sr, the agreement between the calculation and the experiments was poor as shown in Fig. 25. On account of the disagreement, the diffusion coefficients of ^{140}Ba and ^{89}Sr were also obtained from the fractional releases by fitting the calculation to the experiments. In the case of ^{141}Ce and ^{103}Ru, on the other hand, the agreement mentioned above was somewhat good except the release of ^{141}Ce at 1650°C as shown in Fig. 26. Thus, it means that the diffusion coefficients for the release are almost the same to those obtained from the distributions.

From the temperature dependence of the diffusion coefficients as shown in Figs. 27 and 28, Arrhenius equations of the coefficients were obtained and expressed as follows: ^{140}Ba and ^{89}Sr coefficients from the concentration distributions were,

$$D_{Ba} = 7.0\times10^{-3} \exp(-343\times10^{3}/RT) \quad cm^2/sec$$

$$D_{Sr} = 3.8\times10^{-6} \exp(-218\times10^{3}/RT) \quad cm^2/sec,$$

while these coefficients from the releases were the same together as

$$D = 1.2\times10^{-5} \exp(-205\times10^{3}/RT) \quad cm^2/sec.$$

^{141}Ce and ^{103}Ru coefficients from the concentraiton distributions were

$$D_{Ce} = 6.5\times10^{-5} \exp(-251\times10^{3}/RT) \quad cm^2/sec$$

$$D_{Ru} = 2.3\times10^{-3} \exp(-348\times10^{3}/RT) \quad cm^2/sec,$$

where R is a gas constant(=8.314 J/K mol.) and T the absolute temperature(°K).

It is noticed that the coefficients of the alkali-earth fission products(^{140}Ba and ^{89}Sr) obtained from the distributions and the releases are different each other, although the coefficients of ^{141}Ce and ^{103}Ru obtained from the distributions are regarded to be the same as those from the releases. Comparing the concentrations of the alkali earths and two other fission products (Figs. 23 and 24), it is considered that the high concentrations of the former products through the SiC layer compared to ^{141}Ce and ^{103}Ru are caused by the fact that the alkali earth fission products diffuse more easily from the crystal boundaries into the crystal lattice. Therefore, the volume diffusion coefficients of the alkali earth fission products are seemed to be remarkably larger than those of ^{141}Ce and ^{103}Ru in this temperature range.

In the case of ^{141}Ce and ^{103}Ru, it would be certain that the releases are controlled by the boundary diffusion mechanism in this temperature range, because the releases calculated with the diffusion coefficients obtained from the concentration distributions agree to some extent with the experimental results; this implies that almost fission products measured in the concentraion distributions move toward the surface so as to contribute to the releases. Thus, the coeffcients of ^{141}Ce and ^{103}Ru shown above are taken as the boundary diffusion coeffcients. Similarly, the coefficients of the alkali earth fission products from the releases are also taken as the boundary diffusion, but the coefficients from the distributions are apparent because these would express both the boundary- and the volume diffusions.

3.2.2 Releases of gaseous fission products during irradiation

Releases of the gaseous fission products(R/B) from the coated particle fuels are measured in both OGL-1 gas loop and the gas swept capsules. In the case of OGL-1 experiments, the compacts fuels containing 12 % enriched UO_2 were loaded in the 2nd fuel specimen and those containing 20 % enriched UO_2 in the 3rd fuel specimen. Increase of the enrichment in the 3rd fuel is to attain the higher fuel burn-up than in the 2nd fuel.

R/B from the loose coated particles were measured by two capsules, and at present the first swept capsule loading the fuel compacts is under irradiation.

Time dependence of ^{85m}Kr releases from the loose coated particles in the gas swept capsules and the compacts in OGL-1 experiments

are shown together in Fig. 29. Properties of the coated particle fuels used hereon are listed in Table 2. It is characteristic in OGL-1 experiments that R/B values decrease rather rapidly with time at the initial irradiation period. The cause of the decrease, however, is not clear due to few data at present. Comparing R/B values in 2nd and 3rd OGL-1 experiments, it is seen that the latter is about 20 times larger than the former. Difference of these release behavior is obviously caused by different levels of the uranium contamination in the graphite matrix of the compacts. As shown in Table 3, the fraction of the uranium contaminated in the matrix of the compacts in the 3rd experiment is about 45 times higher than that of 2nd experiment.

R/B values from the loose coated particles designated as 74FC1 and 74UC1, both of which are smaller size of the particles than 75FPC4A and 76OPC3 (Table 4), increase gradually with time for short irradiation period, while the values from 75FPC4A and 76OPC3 are almost constant through irradiation.

Temperature dependence of ^{85m}Kr and ^{88}Kr releases from the loose coated particles are shown in Fig. 30. The steady-state release by solid state diffusion from a sphere is given as[14],

$$f_d = \frac{3}{\theta^2}[\theta \coth \theta - 1] \xrightarrow[\theta>2]{} \frac{3}{\theta^2}[\theta - 1] \xrightarrow[\theta>10,]{} \frac{3}{\theta}$$

where

f_d = fractional release rate by diffusion,

$\theta = (\lambda c^2/D)^{0.5}$, dimensionless parameter,

λ = decay constant (sec^{-1}),

D = diffusion coefficient (cm^2/sec)

c = overall radius of coated particles.

Thus, the solid-state diffusion release from the contaminated coatings or the bare kernels is usually expressed as

$$\lambda_i^{0.5} f_i \simeq 3(D/c^2)^{0.5} = \text{constant} \quad \text{(subscript i refers to i'th isotope)}$$

Therefore, $\ln(\lambda_i^{0.5} f_i)$ vs 1/T gives Arrhenius relation as shown in Fig. 30. In the case of 74FC1, two mechanisms of the diffusion releases are noticed. Activation energy in the lower temperature range than 1400°C is about 250×10^3 J/mol. and that in the higher temperature range about 1600×10^3 J/mol.. The former energy fairly agrees with the activation energy of the rare gas diffusion in PyC(255×10^3 J/mol.[15] and 226×10^3 J/mol.[16],both the energies were obtained in HTI-PyC), and therefore, the release below 1400°C is evidently caused by the contaminated uranium in PyC. However, the energy above 1400°C in Fig. 30 is very high, even if the release was originated from the failed particles. For the high activation energy, followings are possible;

(1) change of the failure fraction with irradiation temperature,

(2) change of the physical state of the kernels at the failed particles with irradiation temperature.

Estimation of the failure fraction of the coated particles from R/B values was made tentatively by assuming that the release from the failed particles is equivalent to that from the spherical kernels. This assumption is based on the fact by R. Klersy[17] that R/B values from the bare kernels and the failed particles are not so different each other.

R/B from the loose coated particles was calculated by the code "FECUND"[18] where the releases were occured in the two ways; from

the intact particles and the failed particles. Therefore, the release from the sample, $(R/B)_{total}$, is given as

$$(R/B)_{total} = (1 - f_b)(R/B)_{intact} + f_b(R/B)_{failed}$$

and $(R/B)_{intact}$ is furthermore expressed as

$$(R/B)_{inatct} = (R/B)_{recoil} + (R/B)_{diffusion},$$

where f_b is the failure fraction. $(R/B)_{total}$ is, thus, calcualted as a function of f_b using the proper parameters such as the diffusion coefficients in the coating layers and the kernels, dimensions of the particles, variations of irradiation temperature and fuel burn-up with time , fuel contamination in the coating layers and so on. Comparison of the estimation and the measurements for each sample is shown in Fig. 31 and the main parameters used in calculation are listed in Table 5.

It should be noticed, here, that the recoiled fission products which originate from the contaminated uranium on the surface of the particles or within the recoil range at the outermost coating layer, would reenter into the neighboring particles for the most part, when the loose coated particles are irradiated. Therefore, the gaseous fission products swept out from the loose coated particles are, actually, fairly lower than calcualtion. $(R/B)_{recoil}$ calculated in the code was, thus, corrected by multiplying by a factor which is taken as a fraction of the volumes $(= 1 - V_s/V_t)$, where V_s is the volume of the particles and V_t the volume of the particle holder in the capsule. In Fig. 31, $(R/B)_{recoil}$ calculated with the measured uranium contamination in the outermost PyC layer of each sample is given as a shaded line, where the dimensions and the contaminations

of 74FCl and 74UCl are almost the same together. Then, the temperature dependence of $(R/B)_{total}$ are calculated to the different failure fractions. As shown in Fig. 31, (R/B) of 74FCl and 74UCl at the initial period of irradiation(encircled by dotted lines) are less than 9×10^{-5}, which means that even one coated particle in the sample(about 1.1×10^{4} particles)did not fail, but after 200-400 hrs of irradiation, the failure fractions of both samples rise upto the values between 9×10^{-5} and 2.7×10^{-4} below 1400°C and that of 74FCl is over 2.7×10^{-4} above 1400°C. As already mentioned, however, it is not sure at present whether the rapid increase of (R/B) of 74FCl above 1400°C is due to the increase of the actual failure or due to the change of the physical form of the kernels in the failed particles, that is, from sphere to powder. This will be made clear by PIE of this capsule in the near future.

For calculation of (R/B) of 76OPC3, the uranium contamination at the outermost PyC layer was assumed to be equivalent to the surface contamination of the particles, because the measurements of the contamination of this layer was failed due to very low level. As shown in the figure, (R/B) calcualted with null failure fraction fairly agrees with the measurements. This implies that the coated particles did not fail at this time, although irradiation is continued at present.

In the irradation experiments by OGL-1 and the gas swept capsules, followings are evident:

(1) The release of the gaseous fission products from the small size coated particles(74FCl and 74UCl) are fairly large compared to the large size coated aprticles(76OPC3 and 75FPC4A) due to difference of the contamination at the outermost PyC

layer.

(2) In OGL-1, the release gradually decrease with time from begining of irradiation.

(3) The release greatly depends on the contamination in the matrix of the compacts in OGL-1 fuel specimens.

3.2.3 Migration of solid fission products within/from coated particles

Migration of ^{137}Cs and ^{90}Sr within the coated particles irradiated in JMTR were studied by measuring the concentration distributions in each coating layer. Coating layers were stepwise removed by the following methods; one irradiated TRISO particle was dipped in HNO_3-$K_2Cr_2O_7$ at 140°C for about 10 min. on each solution step to remove the outermost PyC layer, and after removal of the layer, the particle was transferred into KOH-Na_2CO_3 at 800°C to remove the SiC layer. According to the diffusion coefficients of Sr in SiC[19], the temperature, 800°C, for disolution of the SiC layer affects scarcely the concentration distribution in the SiC. After the removal of the SiC layer, the particles were again transferred into HNO_3-$K_2Cr_2O_7$ to remove the inner PyC layer. During the solution of the inner PyC, most of the particles were broken due to the inner pressure of CO and the gaseous fission products. Fig. 32 shows the typical X-ray microradiographs of the coated particles at several steps of the removal process. Variation of the layer thickness was measured by the X-ray microradiography and the typical result is shown in Fig. 33.

Measurements of the concentration profiles of ^{137}Cs and ^{90}Sr were made in the coated particles irradiated under several different conditions as listed in Table 6. Results of the concentration profiles of these fission products are shown in Fig. 34(a and b). In the figure, the layer thickness is based on the interface between the outer PyC and the SiC layers due to the different dimensions of the particles. It is seen in Fig. 34(a) that ^{137}Cs concentration is minimum at the interface of the outer PyC and the SiC layers; all of the concentration profiles in the outermost PyC rise toward the surface of the particles and those in the SiC layer toward the inside.

As seen in Fig. 34(b), on the other hand, the concentration profiles of ^{90}Sr are relatively flat through the outermost PyC layer, but two features on the concentration are clear in this layer. The coated particles showing the high concentration($\sim 10^{-2}$) in the layer were irradiated at high temperature above 1400°C and those showing the low concentration($\sim 10^{-5}$) at low temperature such as 1140°C, although Sample 1-B is stepwise annealed from 1200° to 1800°C after irradiation.

Difference in the behaviors of ^{137}Cs and ^{90}Sr in the SiC layer is not distinguished in these profiles. Although the concentration of ^{137}Cs in the SiC layer of Sample 2 is low compared to that of ^{90}Sr, this would be due to the low concentration in the inner PyC layer. Comparing the profiles of Sample 2 and others, it is seen that the gradient of the profile of both of the fission products is affected by the density of the SiC layer; the gradient of Sample 2 which has the low density SiC layer(Table 6), is gentle, while the others are steep.

Releases of both of the fission products by stepwise annealing from 1200° to 1800°C are shown in Fig. 35. In the figure, ^{90}Sr

fractional release is above one order of magnitude higher than that of ^{137}Cs at every temperature tested. Although the fractional release of ^{90}Sr increases rapidly at 1800°C, probably, due to the release from the kernel, that of ^{137}Cs dose not show this behavior. This imply that the diffusion coefficient of ^{137}Cs in the SiC layer is smaller than that of ^{90}Sr. According to the review by Zoller[5], the diffusion coefficients of Sr in LTI-PyC is about three orders of magnitude larger than that of ^{137}Cs at 1400°C, and therefore, considering the above release behaviors, it would be suggested that Sr release from TRISO coated particles is predominantly controlled by the SiC layer as already reported[21], but that of Cs, by the PyC layer as well as the SiC layer.

From the study of Cs and Sr migrations in the coated particles, followings are found:

(1) At the outermost PyC layer of irradiated particles, Cs concentration increases toward the surface.

(2) Gradient of the profile in the SiC layer is affected by the density of the SiC; low desity SiC makes the gentle gradient.

(3) From the profiles in the SiC layer, difference of the diffusions of Cs and Sr is not distinguished clearly.
From the measurements of the release, it is suggested that the release of Cs is controlled also by the PyC layers as well as the SiC layer in TRISO particles.

4. Summary

Irradiation performances and their principal results concerning to the coated particle LEU fuels were described. JAERI's irradiation-experiments for development of VHTR fuels were made in use of JMTR and JRR-2. In JMTR, the closed capsules, the gas swept capsules and OGL-1 were available to test the coated particle fuel under irradiation.

With regard to the irradiation results on the kernels, the typical features such as the kernel shrinkage, the kernel migration, the kernel viscous flow into the cracked buffer layer and the precipitation of the solid fission products at the nodal points of the grain boundaries were observed.

OPTAF of PyC layers of the irradiated TRISO particles were measured and it was found that OPTAF values increased with fast neutron fluence and irradiation temperature. Also, concerning to the effects of the anisotropy on PyC stability, it was found that anisotropy factor(BAF) was desirable to be less than 1.04 because of the residual stress.

Crushing strength of unirradiated and irradiated coated particles was measured. The results showed that both of the layer and the kernel crushing strength decreased up to about 50 % with increase of fast neutron fluence to 1×10^{21} n/cm^2 ($E > 0.18$ MeV) and burnup to 2 %FIMA.

Diffusion coefficients of the fission prodcuts in the slightly irradiated SiC were obtained by measuring the releases and the concentration distributions in the SiC layer. Xe diffusion coefficients obtained by the releases from the recoiled SiC powder and from SiC coated particles are the same together. The coefficients of the

solid fission products such as ^{89}Sr, ^{140}Ba, ^{141}Ce and ^{103}Ru were obtained by the concentration distributions in the layer and the releases from the SiC coated particles.

The release results of the gaseous fission products from TRISO coated particle fuels obtained in OGL-1 and the gas-swept capsules are presented. Then, the failure fractions were tentatively calculated from the releases obtained in the gas-swept capsules.

The concentration distributions of ^{137}Cs and ^{90}Sr in the irradiated TRISO coated particles were measured. It was found that Cs concentration distributions showed the steep gradient toward the surface in the outermost PyC layer. It was shown that the Cs release from the TRISO particle was remarkably less than the Sr release, probably, due to the lower diffusion coefficient of Cs in the PyC than Sr.

Acknowledgement

The authors wish to express their thanks to their colleagues of the Fuel Irradiation and Analysis Laboratory, Division of Nuclear Fuel Research,for their helps in the irradiation experiments, and to Dr. J. Shimokawa, Head of the division, for his interest and encouragement. Thanks are also due to Mr. K. Ishimoto, Chief of Tokai Hot Laboratory, and his coleagues for their great aid in PIE, and due to Dr. S. Oouchi, Head of Division of JMTR, and his colleagues for their irradiation work.

References

[1] T.Arai, Pernsonal communication(1980).

[2] T.Aochi, J.Shimokawa et al, Japan Atomic Energy Research Institute Report JAERI-M 6845(1977).

[3] O.Baba, Personal communication on STPDSP2 code(1980).

[4] L.G.Wisnyi and S.W.Pijanowski, KAPL-1702(1957),cited in "Uranium dioxide"(J.Belle, Naval Reactors, Division of Reactor Development,USAEC).

[5] P.Zoller, KFA report JUL-1324(1976).

[6] P.E.Brown and R.L.Faircloth, J. Nucl. Mater., 59(1976)29.

[7] H.Nabielek, P.E.Brown and P.Offerman, KFA report JUL-1407 (1977).

[8] J.C.Bokros and K.Koyama, J. Appl. Phys., 41(1970)3146.

[9] D.P.Harmon and C.B.Scott, Nucl. Technol., 35(1977)343.

[10] D.N.Morison, R.H.Barnes, T.S.Elleman and D.N.Sundermann, Battelle Memorial Institute report BMI-1592(1962).

[11] K.W.Baurman, KFA report JUL-685-PA(1970).

[12] P.L.Farnsworth and R.L.Coble, J.Amer. Ceram. Soc., 49(1966) 264.

[13] R.N.G.Tagore, cited in Ref.[12].

[14] J.W.Prados and J.L.Scott, Oak Ridge National Laboratory repor ORNL-3421(1963).

[15] K.Fukuda and K.Iwamoto,J.Nucl.Sci.Technol.,12(1975).

[16] B.Chinaglia, G.Mosca and H.Walther, EURATOM report EUR4951e (1973).

[17] R.Klersy, A.Schurenkamper and O.Sisman, EURATOM repor EUR 5363e (1975).

[18] M.Makino and S.Yasukawa, Japan Atomic Energy Research Institute report JAERI-M 4883(1972),"FECUND" is amended by S.Mitake thereafter.

[19] Gulf General Atomic report GA-8662(1968).

[20] Gulf General Atomic Report GA-8367(1968).

Table 1 Fuel specifications by First Conceptional Design

Kernel	Enrichment		2, 4, 6
	Material		UO_2
	Diameter (um)		600
Coated particle	Coating thickness (um)	1st layer (buff. PyC)	60
		2nd layer (PyC)	30
		3rd layer (SiC)	25
		4th layer (PyC)	45
	Particle diam. (um)		920
Fuel compact	Dimension (mm)	Outer diam.	36
		Inner diam.	18
		Length	36
	Particle loading (v/o)		30
Fuel pin	Graphite sleeve dimension (mm)	Outer diam.	46.0
		Inner diam.	36.2
		Length	555
	Number of compacts		15
Fuel block	Graphite block dimension (mm)	Across-flat diam.	299
		Height	570
	Number of fuel pin		12

Table 2 Main Specifications of the OGL-1 Gas Loop

Primary Coolant	
Gas	Helium
Pressure	35 kg/cm^2G (Max.)
Temperature	1000°C (Max.)
Flow	100 g/sec (Max.)
Neutron Flux	
Fast	$9x10^{12}$ nv (>1 Mev)
Thermal	$6x10^{13}$ nv (<0.625 ev)
Nuclear Heat Generation of Specimen	135 kW (Max.)
Size of Specimen	80mmφx750mml (Max.)

Table 3 Uranium contamination in the fuels for 2nd and 3rd OGL-1 experiments

Uarnium contamination		Fuels for 2nd experiment		Fuels for 3rd experiment	
		Contamination	Fraction	Contamination	Fraction
Surface contamination of coated particles (μg/g particles)		2.0	3.2×10^{-6}	2.3	3.6×10^{-6}
Compacts	Leaching	10		5	
	Solution of disintegration	1825		13	
	Graphite powder	86		10	
	Total (μg/ a compact)	1921	9×10^{-5}	28	2×10^{-6}

Table 4 Characteristics of the samples in the gas swept capsules and OGL-1

Irradiation experiment		74F-9J		75F-4A			2nd OGL-1	3rd OGL-1
Sample		74FC1	74UC1	75FPC4A	76FPC1	76OPC3	Compacts	Compacts
Kernel	Material	UO_2	UO_2	UO_2	UO_2	UO_2	UO_2	UO_2
	Enrichment (%)	8	8	4	4	12	12	20
	Mean diam. (μm)	493	495	617	602	599	581-603	592
Coating type		TRISO	TRISO	TRISO	TRISO	TRISO	TRISO	TRISO
Mean particle diam. (μm)		765	790	911	890	895	886-895	898
Compacts	Outer diam. (μm)						24	36
	Inner diam. (μm)						8	18
	Length (μm)						36	36
Uranium content in a sample (g)		6.6	6.2	10.5	10.5	10.5	737	429

Table 5 Main parameters used for FECUND code

Sample		74FC1 74UC1	760PC3
Uranium contamination in outer PyC layer (g uranium in PyC/ g uranium in Kernel)		1.1×10^{-4}	3×10^{-7}
Radius of kernels (μm)		247	299
Thickness (μm)	Buffer PyC	43	59
	Inner PyC	32	30
	SiC	28	26
	Outer PyC	42	45
Diffusion coefficients	UO_2	$D = 3\times10^{-2}\exp(-264\times10^3/RT)$	
	Buffer PyC	$D = 1\times10^{-7}\exp(-42\times10^3/RT)$	
	Inner PyC	$D = 2.9\times10^{-5}\exp(-255\times10^3/RT)$	
	Outer PyC	$D = 2.9\times10^{-4}\exp(-255\times10^3/RT)$	
		(cm^2/sec)	
		R = 8.314 J/°K	

Table 6 Characterization and irradiation conditions of coated particles

		Sample 1-A[a]	Sample 1-B[a]	Sample 1-C[a]	Sample 2
Kernel:	Material	UO_2	UO_2	UO_2	UO_2
	^{235}U enrichment (%)	20	20	20	8
Buffer PyC:	Density (g/cm^3)	1.21	1.21	1.21	1.18
	Thickness (μ)	43	43	43	39
Inner PyC:	Density (g/cm^3)	1.76	1.76	1.76	1.80
	Thickness (μ)	34	34	34	26
SiC:	Density (g/cm^3)	3.19	3.19	3.19	3.15
	Thickness (μ)[b]	28.7	31.0	29.6	33.7
Outer PyC:	Density (g/cm^3)	1.76	1.76	1.76	1.9
	Thickness (μ)[b]	43.5	39.2	44.5	48.2
Irradiation condition Temperature (°C)		mean 1140 (1170–1100)		1560–1495	1460–1200
Time (days)		30.3		12.1	12.1
Fuel burn up (% FIMA)		2.02		0.7	0.13
Fast neutron dose (n/cm^2, $E > 1.0$ MeV)		5×10^{19}		6×10^{18}	4×10^{19}
Reactor		JMTR		JRR-2	JRR-2

a) Taken from same batch of coating operation.
b) Measured for individual particle by X-ray microradiography.

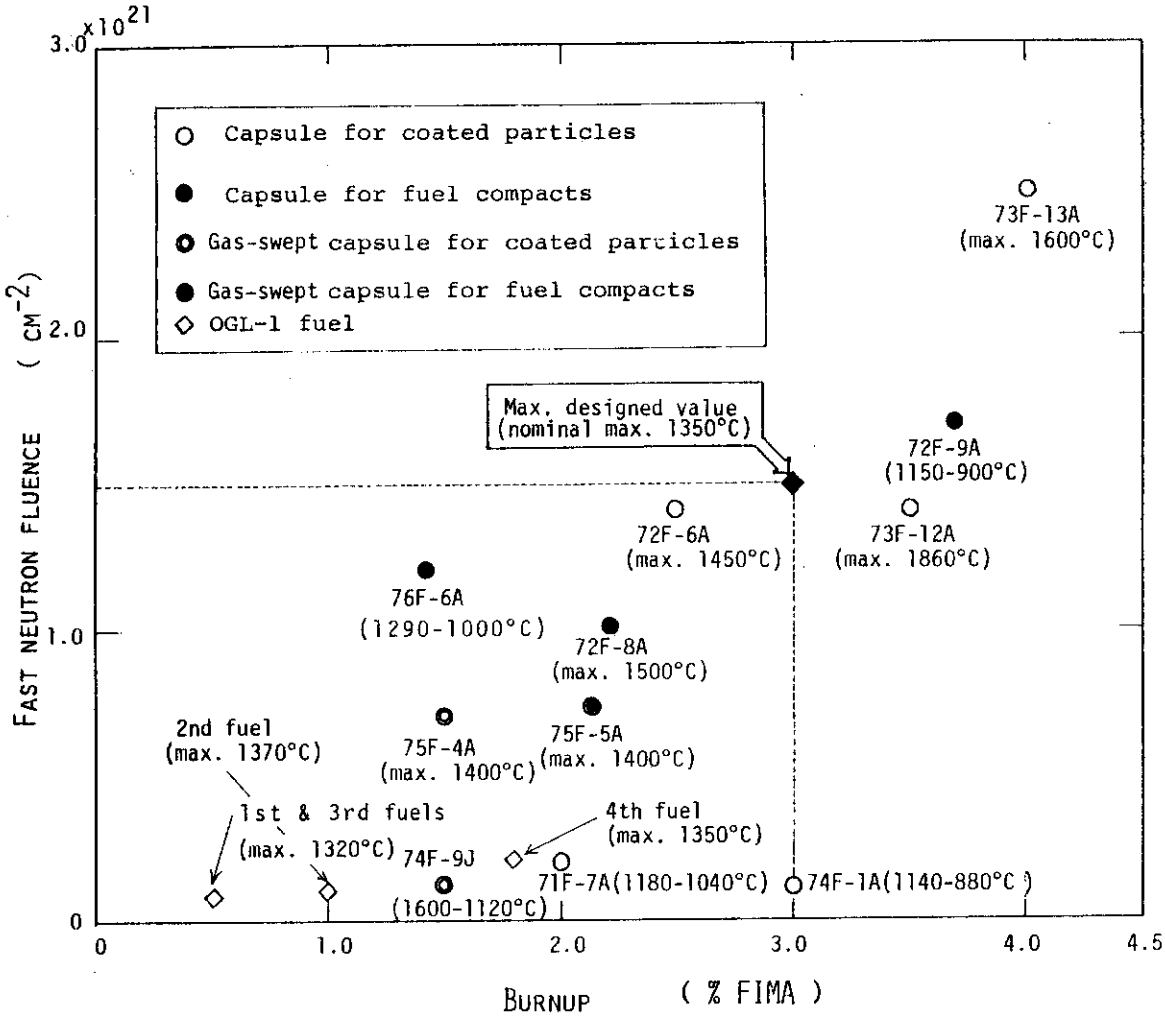

Fig. 1 Irradiation experiments in JMTR.

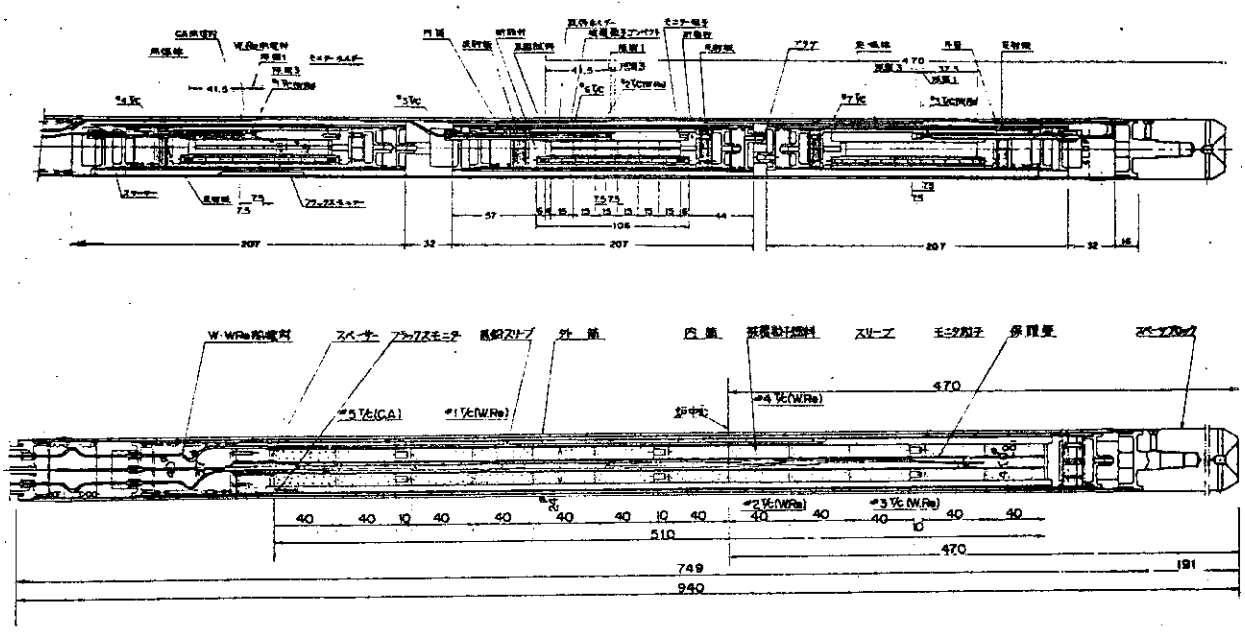

Fig. 2 Irradiation capsules of JMTR.

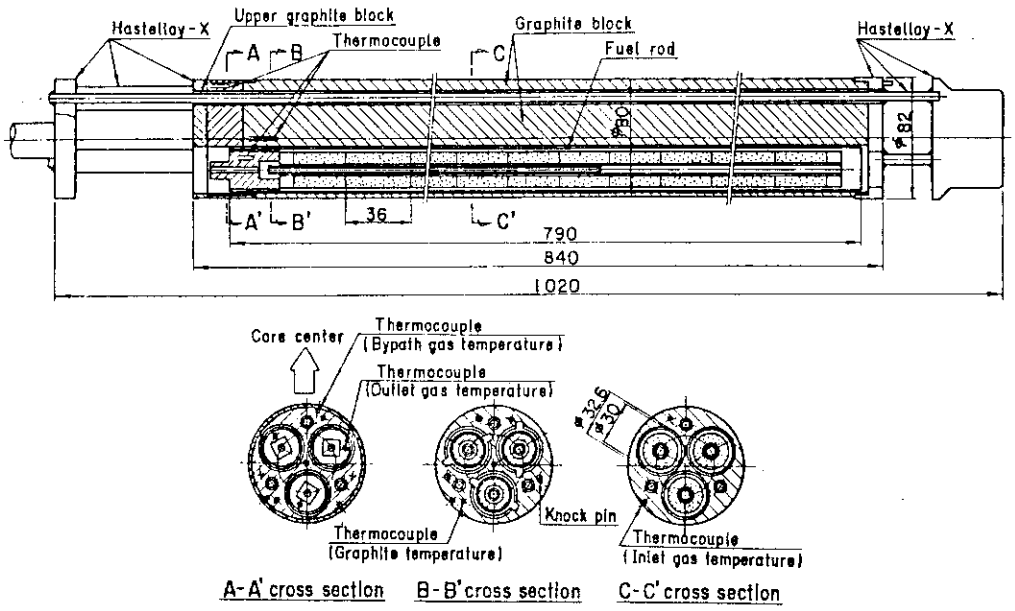

Fig. 3 OGL-1 fuel specimen.

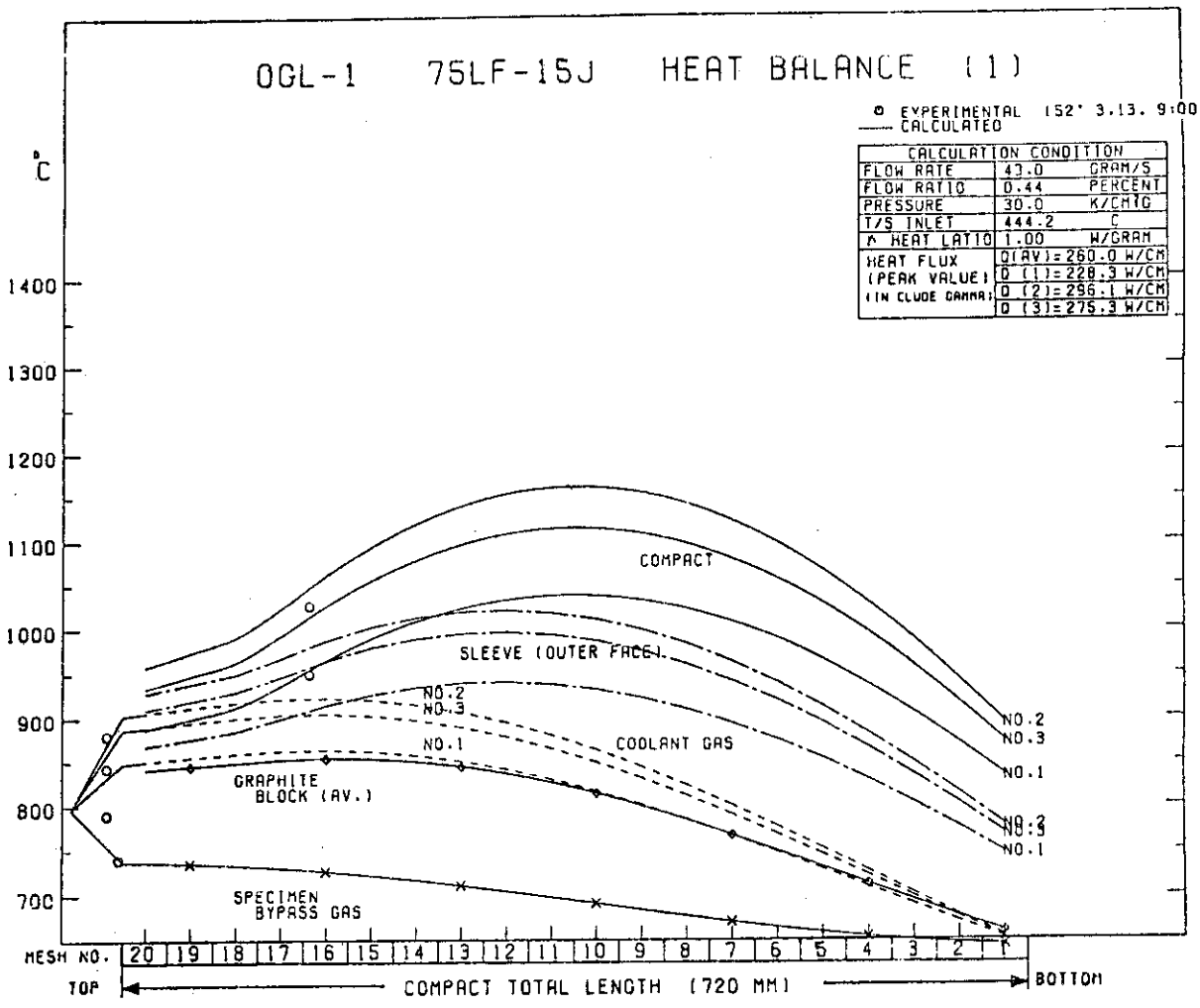

Fig. 4 Temperature distributions along axial directions calculated and measured in OGL-1 fuel specimen.

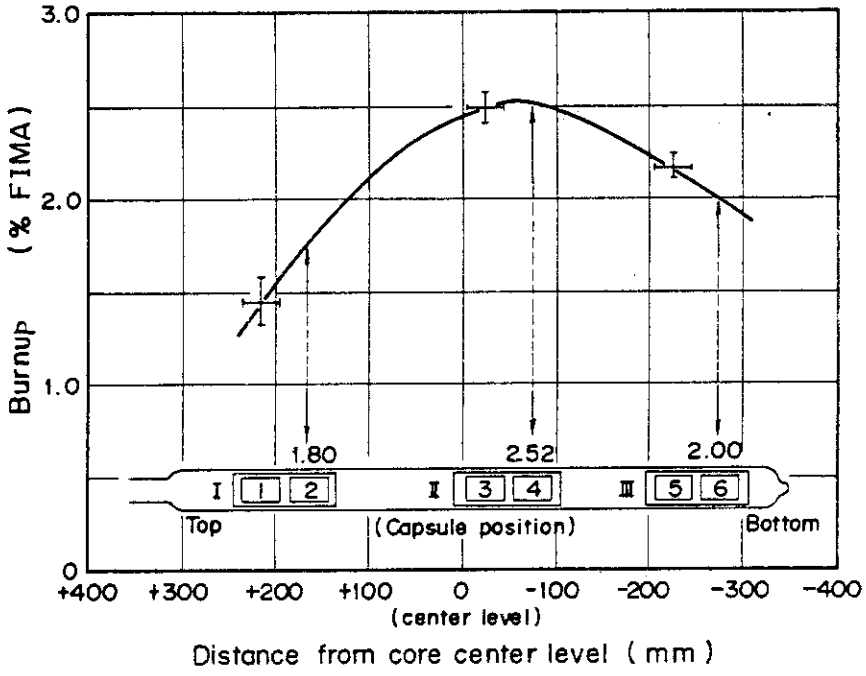

Fig. 5 Burnup distribution in Capsule 72F-6A.

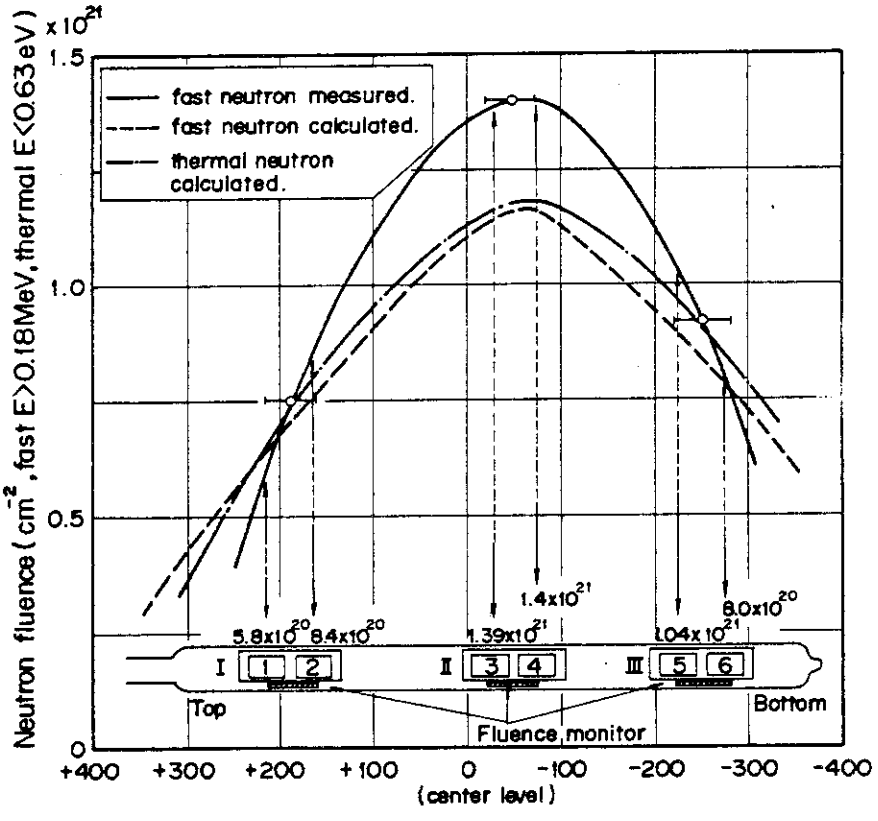

Fig. 6 Neutron fluence distribution in Capsule 72F-6A.

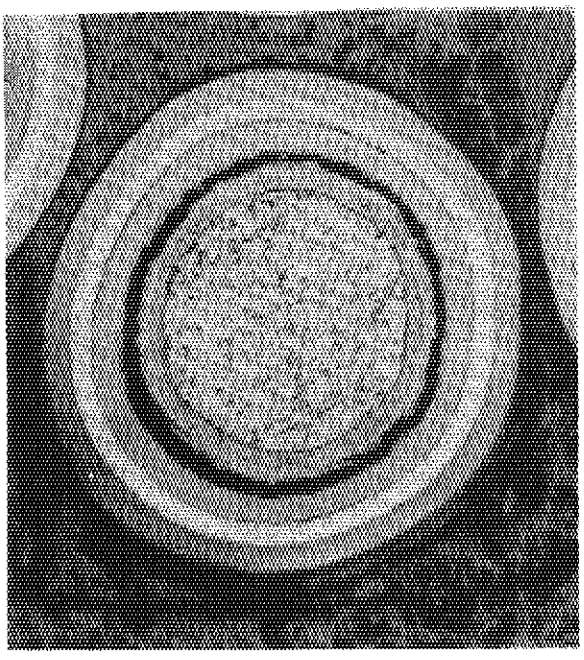

Fig. 7 Kernel shrinkage observed frequently in the particles with low density kernels(90%TD). (2 %FIMA, 1170-790°C, $1x10^{21}$ n/cm^2 (E > 0.18MeV) of fast neutron fluence)

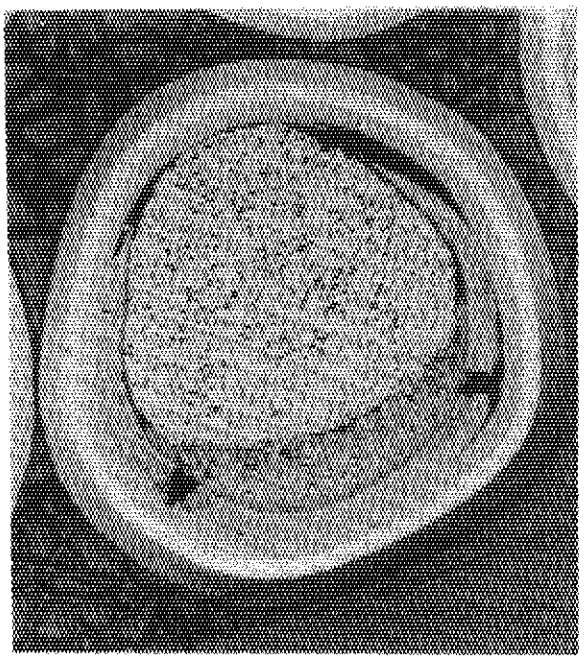

Fig. 8 Typical example of the kernel migration in the particle irradiated by Capsule 73F-12A.

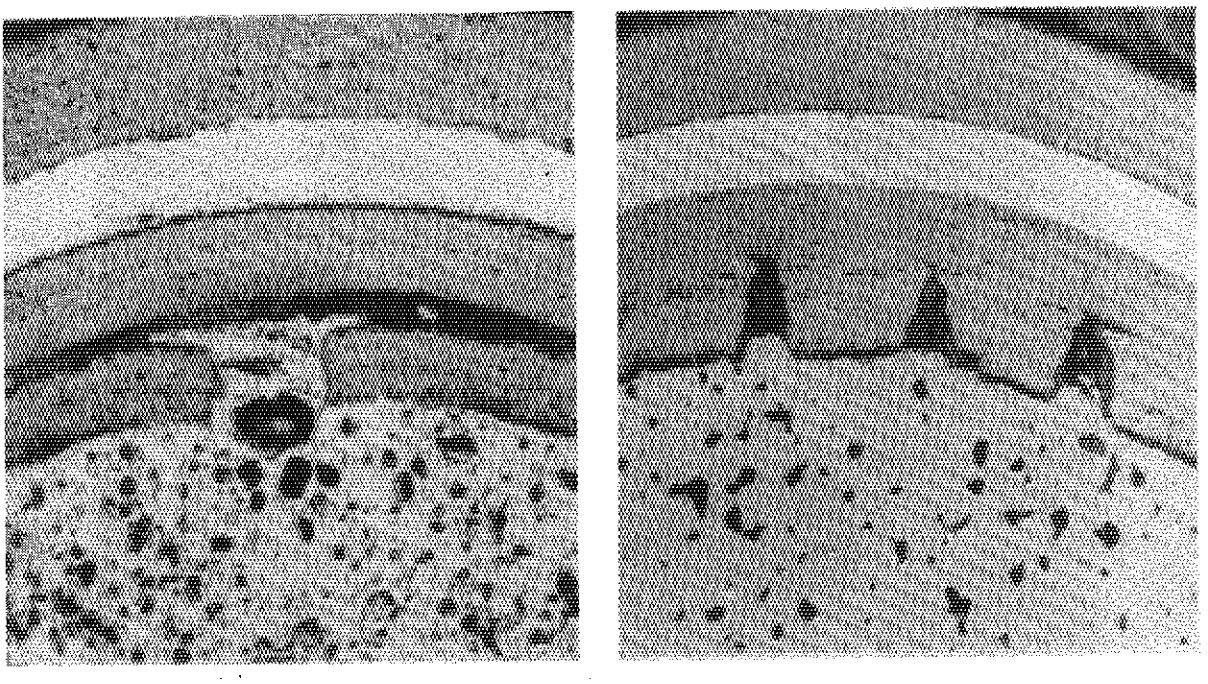

Fig. 9 Kernel viscous flow in the particles irradiated upto 1.9 %FIMA at 1190-1070°C(left) and upto 3.0 %FIMA at 1500-1000°C(right).

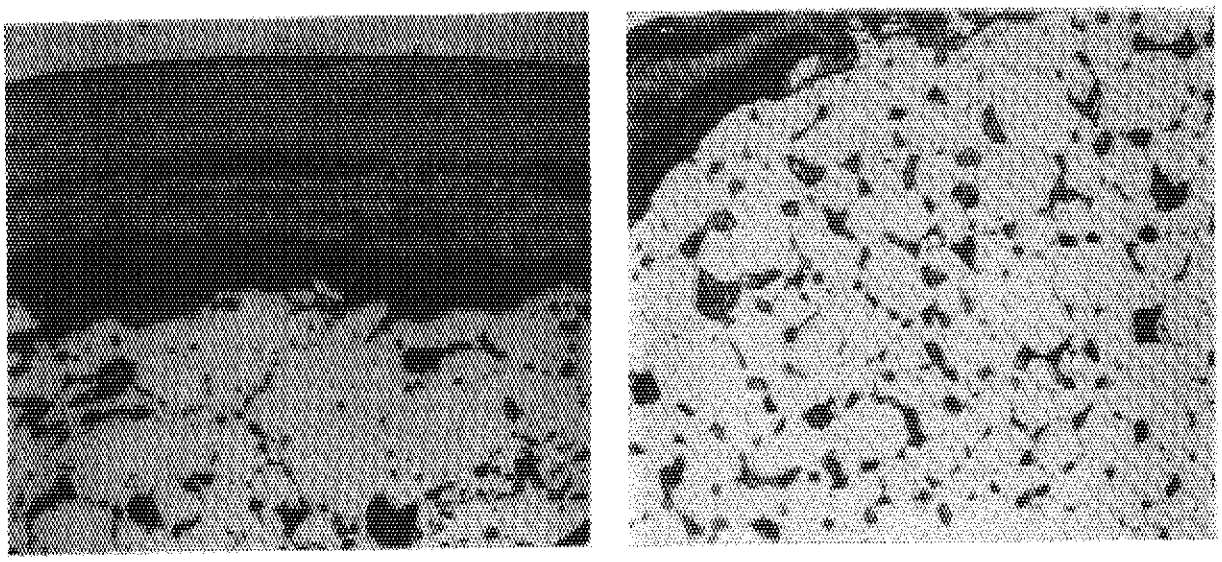

Fig. 10 Fission-product precipitation at the grain boundaries of the kernels. [upto 2 %FIMA at 1240-1120°C(left) and upto 3 %FIMA at 1500-1000°C].

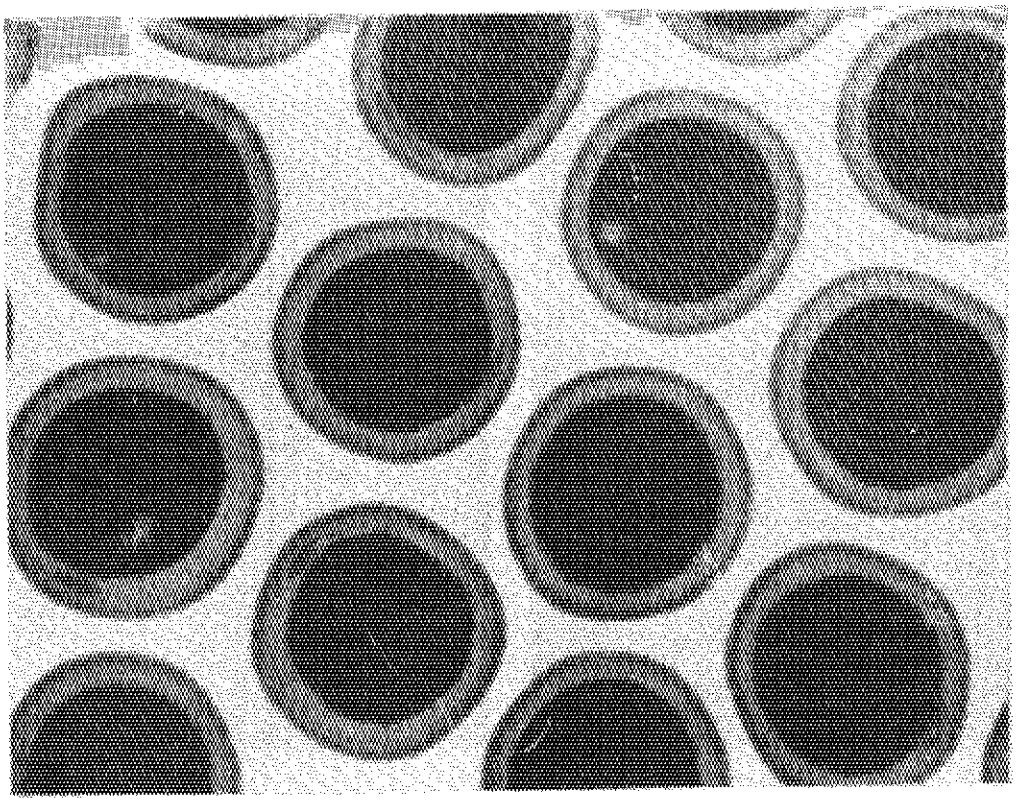

Fig. 11 X-ray microradiograph showing fission-product segregation (darkness at the buffer layer). The particles were irradiated upto 2.5 %FIMA, 1.4×10^{21} n/cm^2 (E >0.18MeV) at 1370-1230°C.

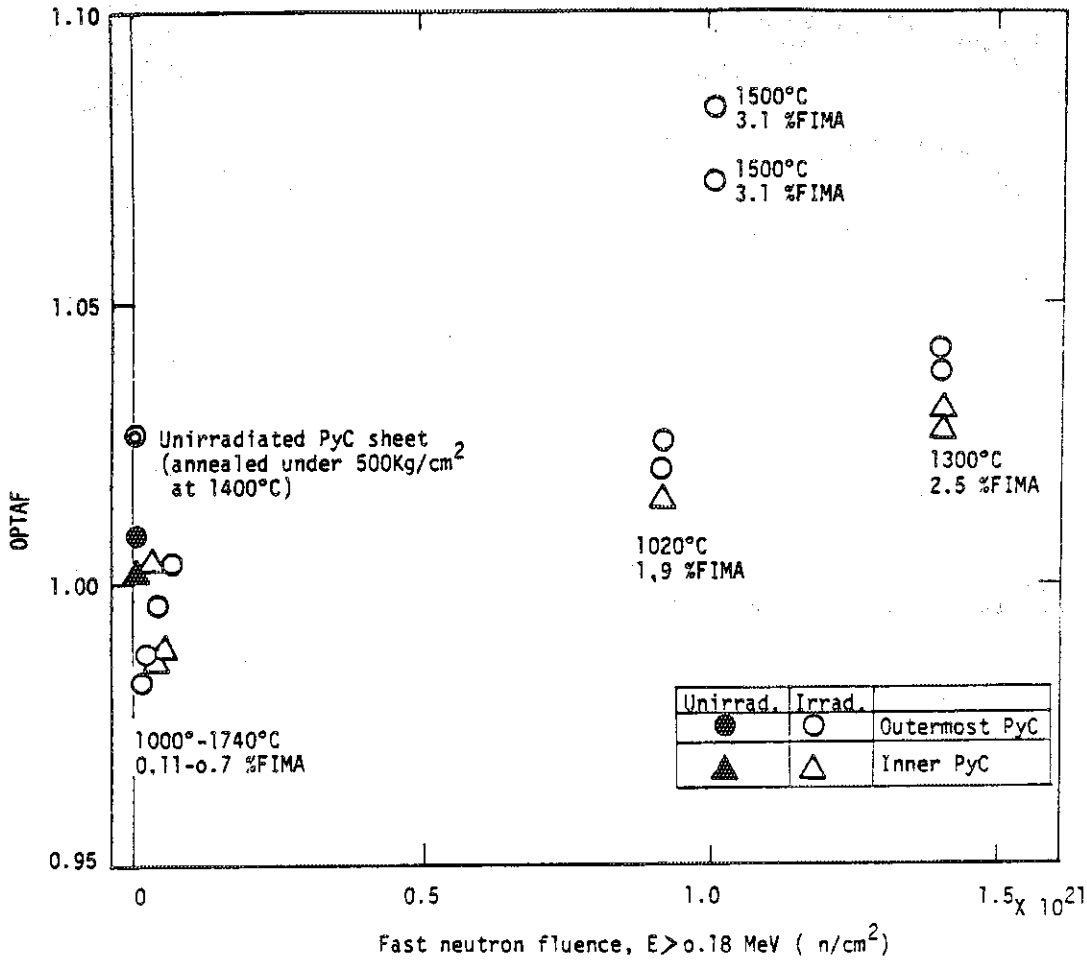

Fig. 12 OPTAF variation with fast neutron fluence.

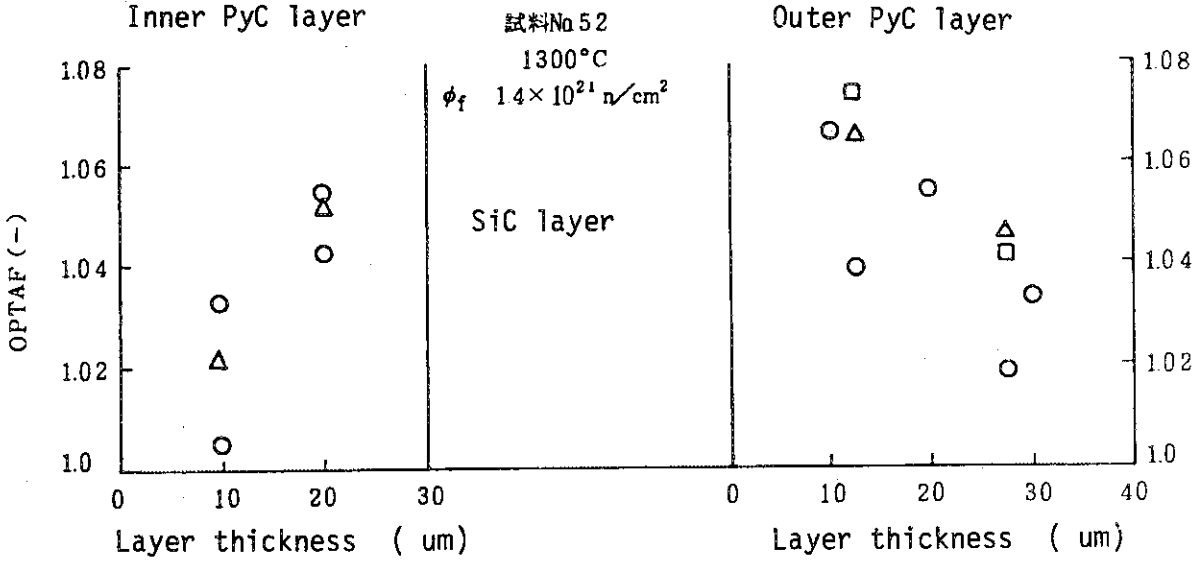

Fig. 13 Variation of OPTAF values inside the inner and outer LTI PyC layers.

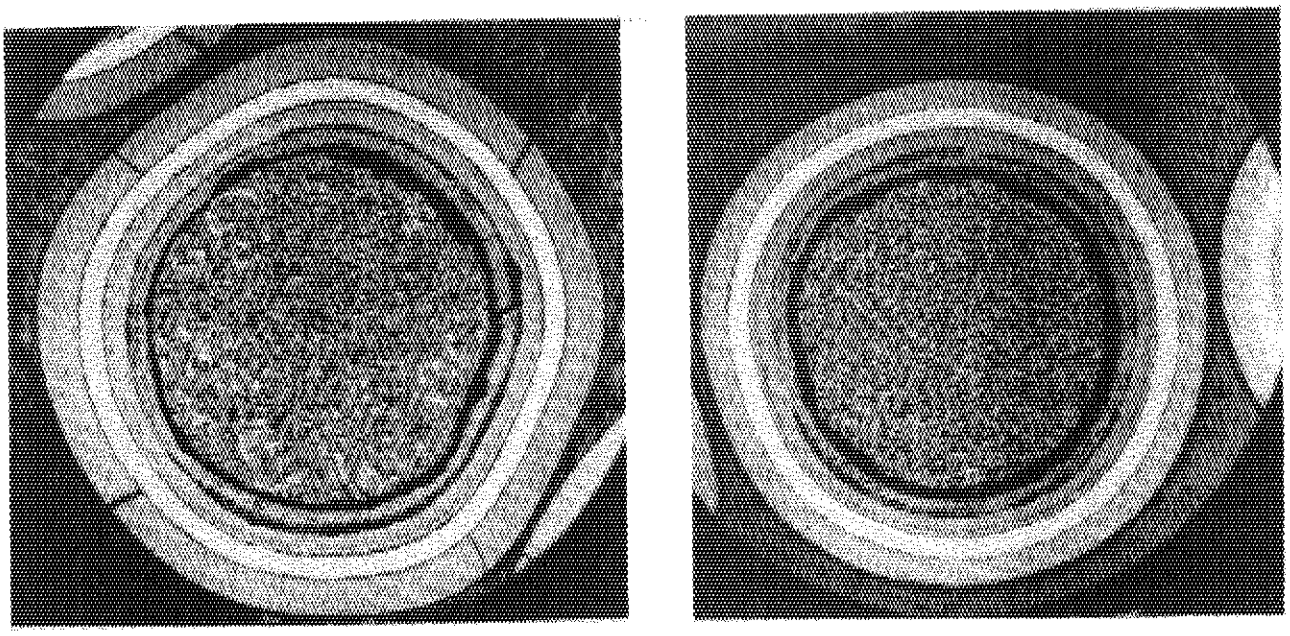

Fig. 14 Radially cracked outer PyC layer(BAF 1.26) and crack-free PyC layer(BAF 1.03). The cracks were formed during polishing in PIE. The former particles were irradiated to 0.9×10^{21} n/cm^2 at 1100°C and the latter, 0.7×10^{21} n/cm^2(E 0.18MeV) of fast neutron fluence at 1000°C.

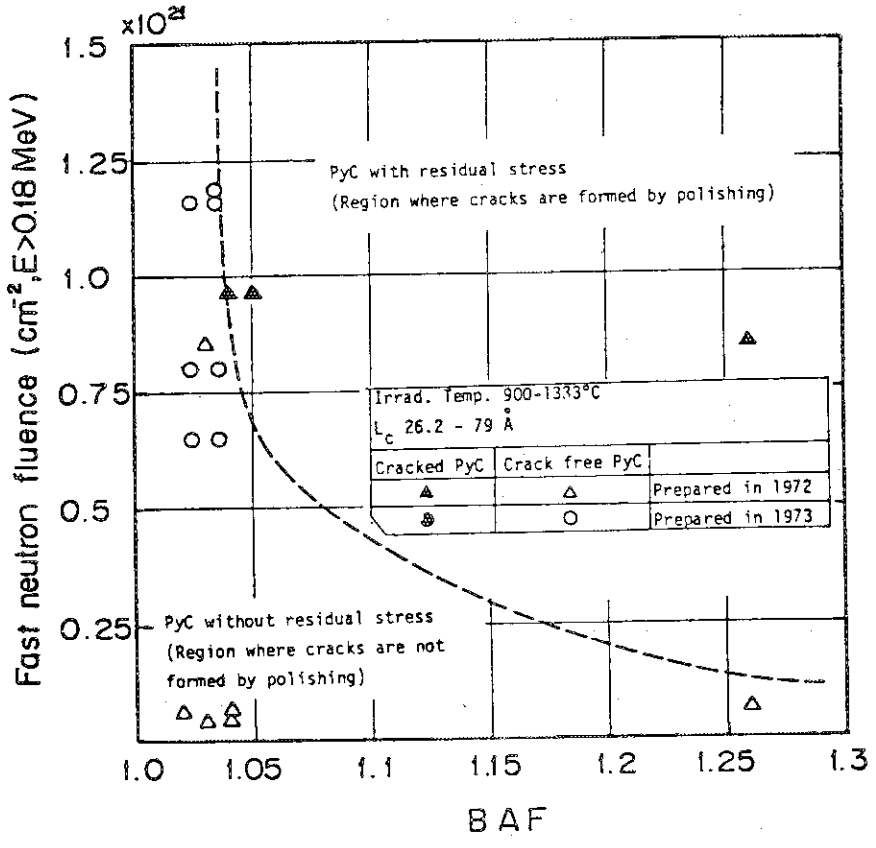

Fig. 15 Influence of BAF at the outer PyC layer on the layer stability by irradiation.

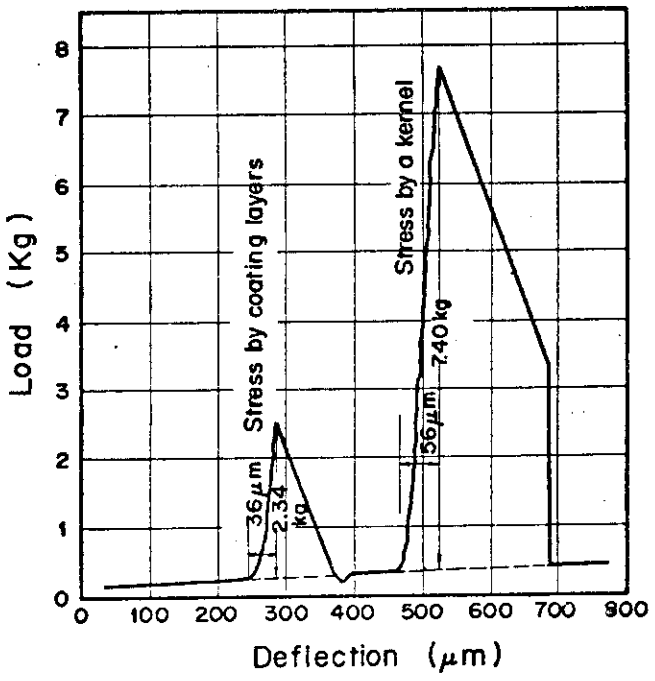

Fig. 16 Load-deflection curve of irradiated coated particle.

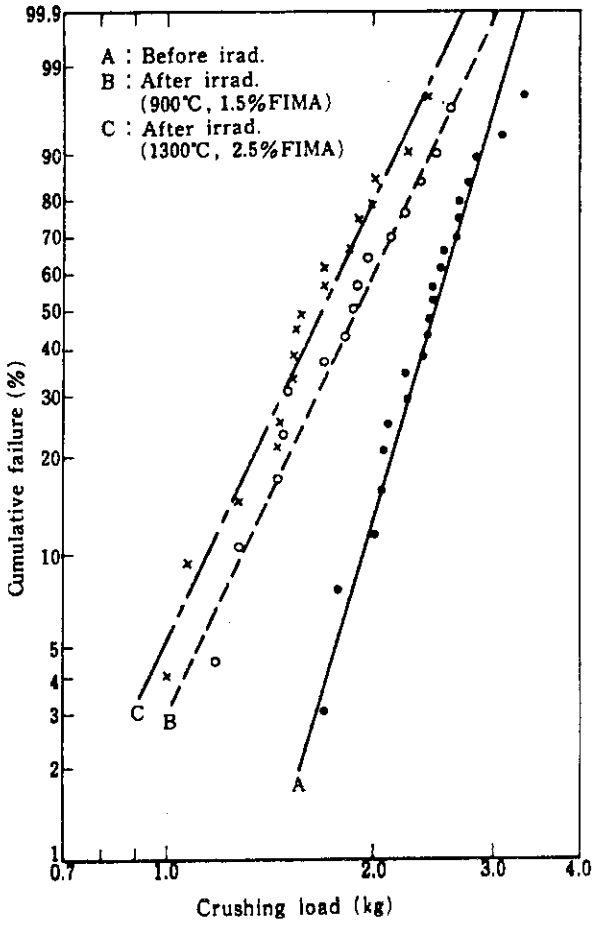

Fig. 17 Weibull plots of unirradiated and irradiated particles.

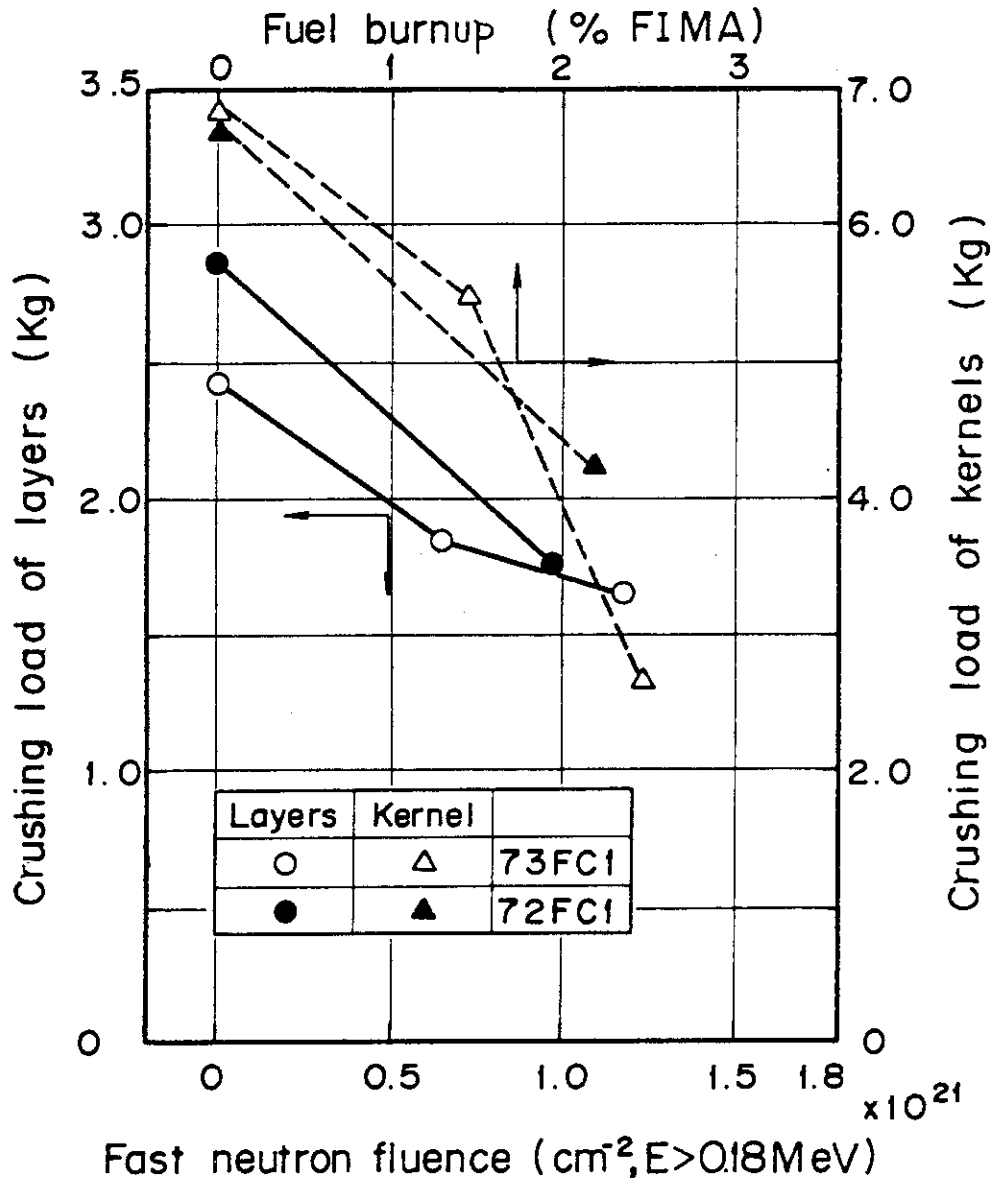

Fig. 18 Variation of crushing load with irradiation conditions.

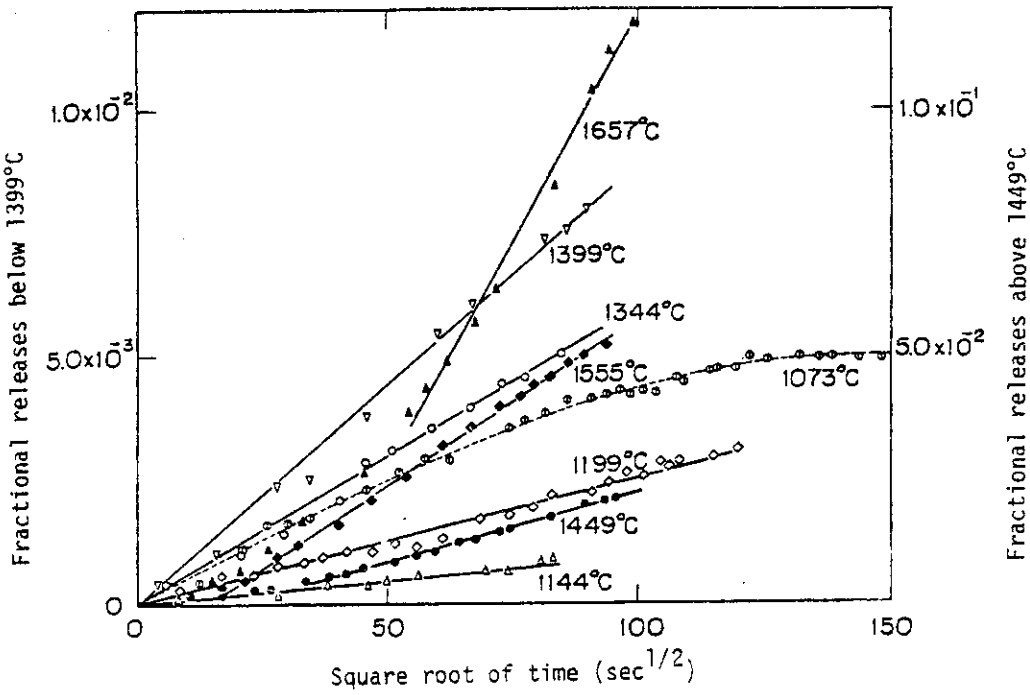

Fig. 19 Fractional releases of ^{133}Xe under stepwise heating.

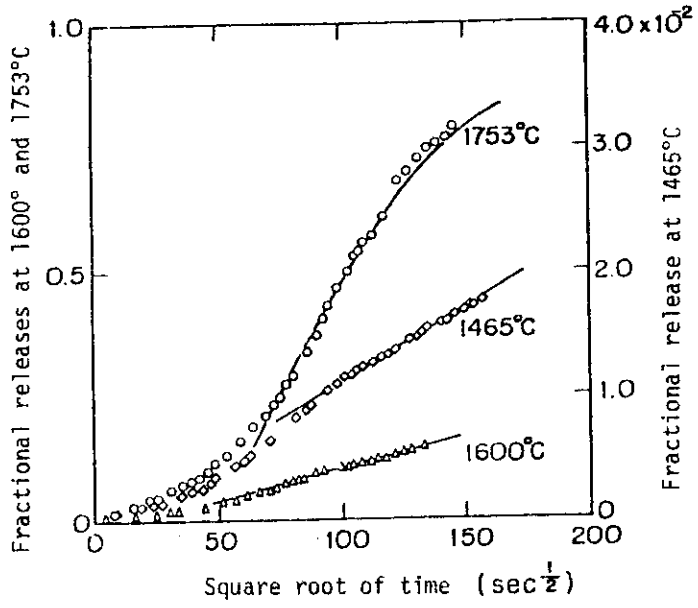

Fig. 20 Fractional releases of ^{133}Xe under isothermal heating.

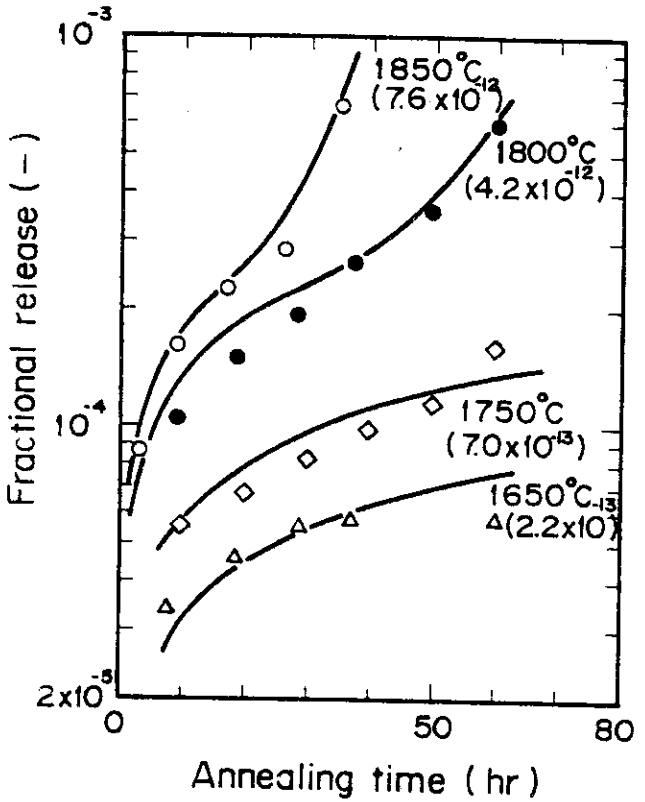

Fig. 21 Fractional release of ^{133}Xe from SiC coated fuel particles; solid lines indicate results of calculation, and numbers in parentheses diffusion coefficients (cm^2/sec).

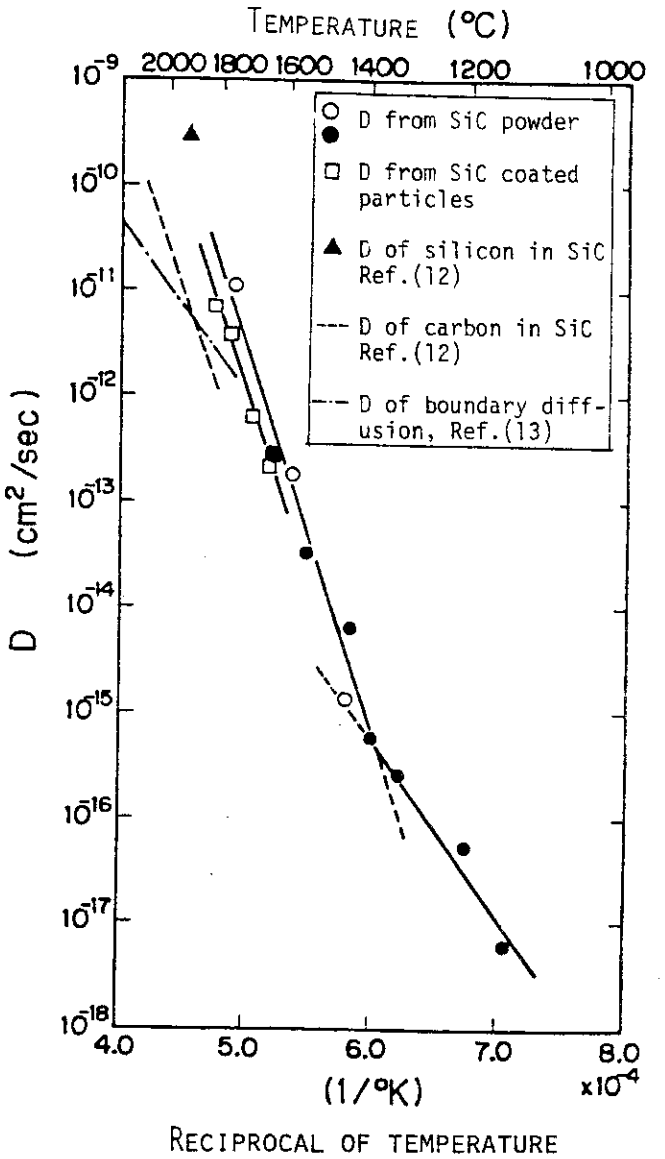

Fig. 22 Temperature dependence of ^{133}Xe diffusion coefficients in SiC.

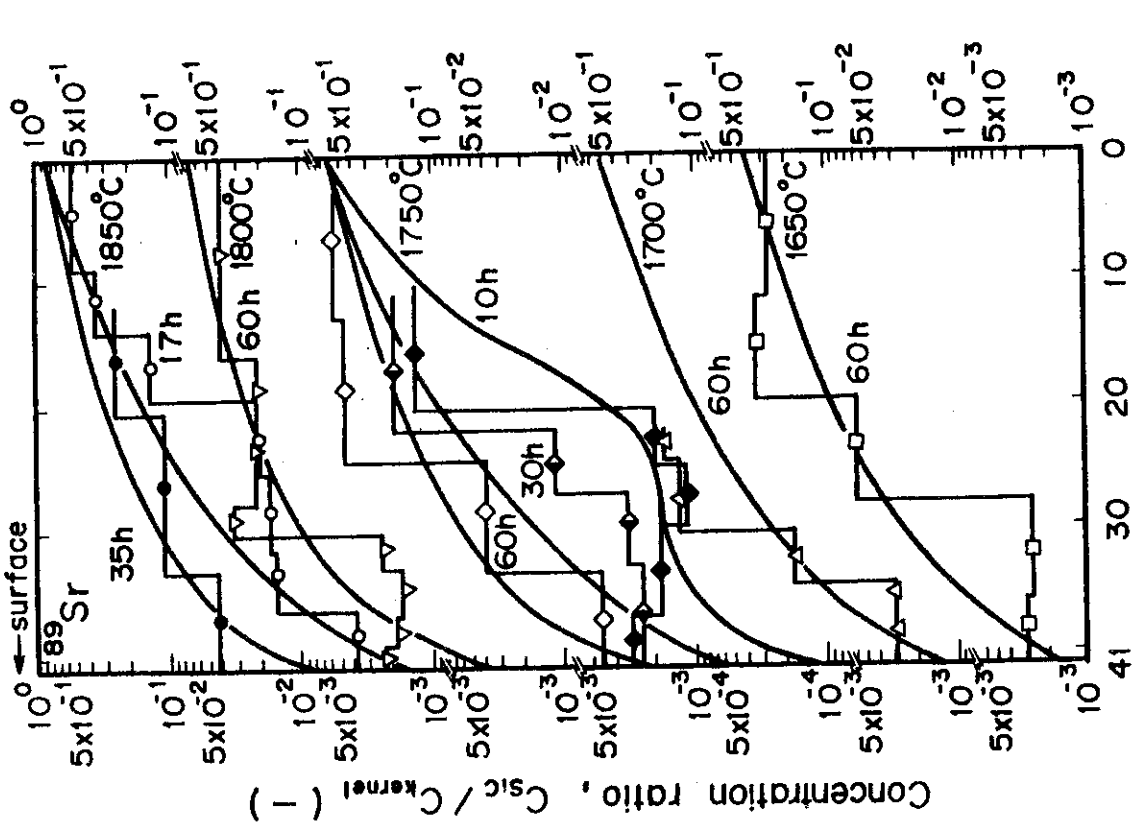

Fig. 23 Concentration distributions of ^{89}Sr in the SiC layer; annealing temperature and its time are shown near respective solid line indicating results of best fitting calculation.

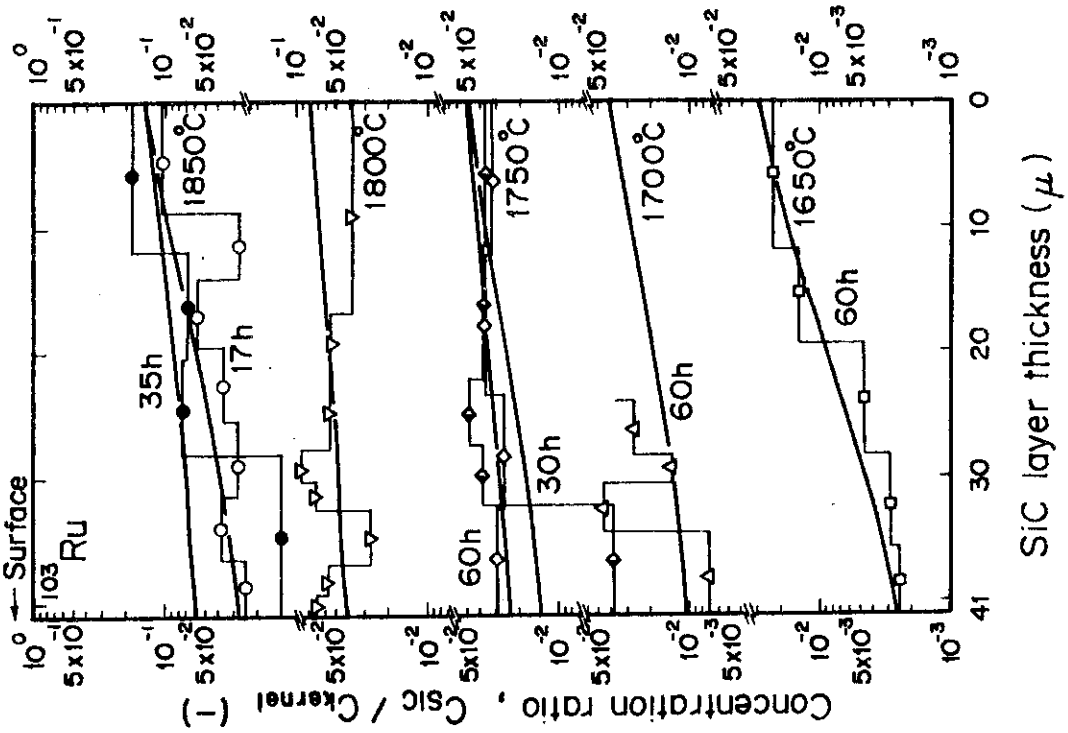

Fig. 24 Concentration distributions of ^{103}Ru in the SiC layer; annealing temperature and its time are shown near respective solid line indicating results of best fitting calculation.

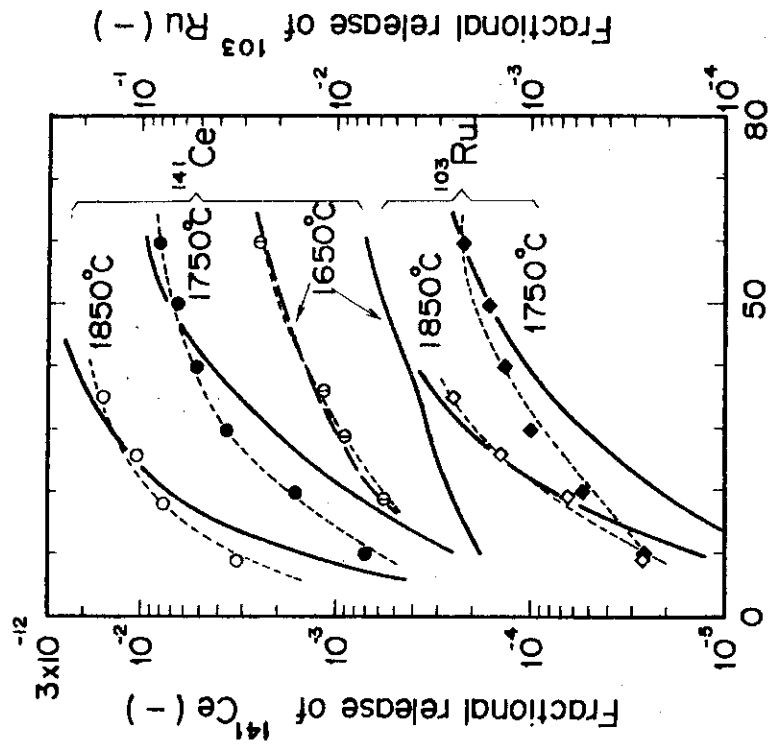

Fig. 26 Fractional releases of ^{141}Ce and ^{103}Ru versus annealing time; dotted, solid and broken lines indicate results of experiment, calcualtion using parameters obtained in distribution analysis and best fitting calculation to the experiment, respectively.

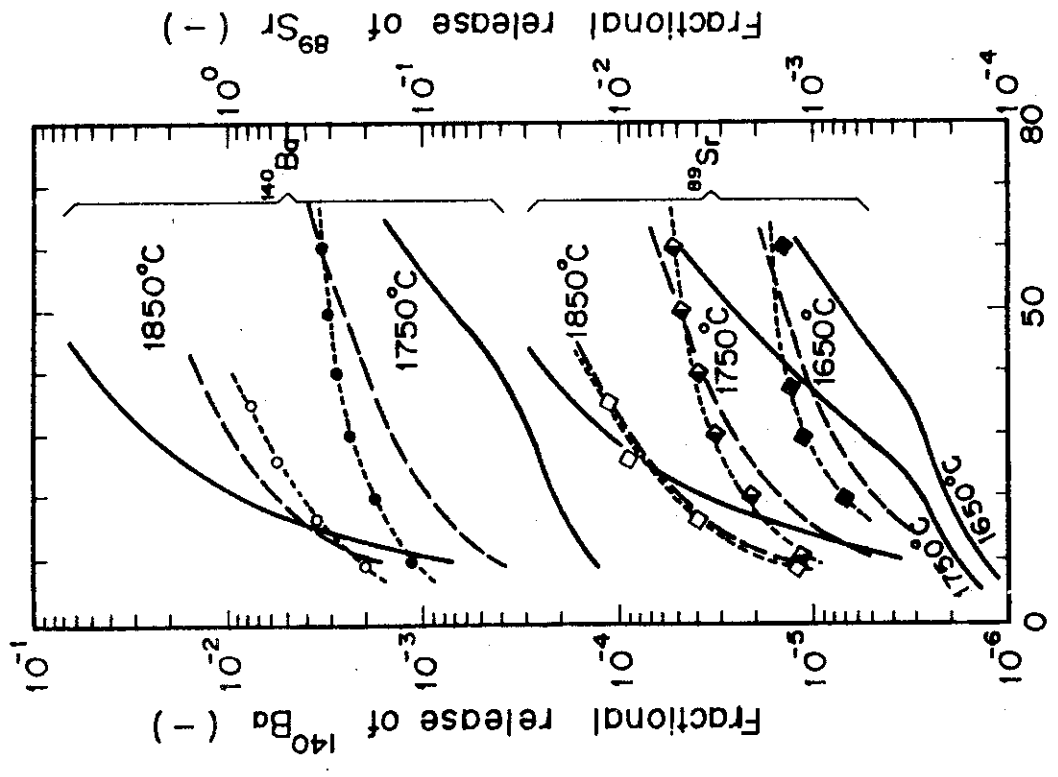

Fig. 25 Fractional releases of ^{140}Ba and ^{89}Sr versus annealing time; dotted, solid and broken lines indicate results of experiment, calcualtion using parameters obtained in distribution analysis and best fitting calculation to the experiment, respectively.

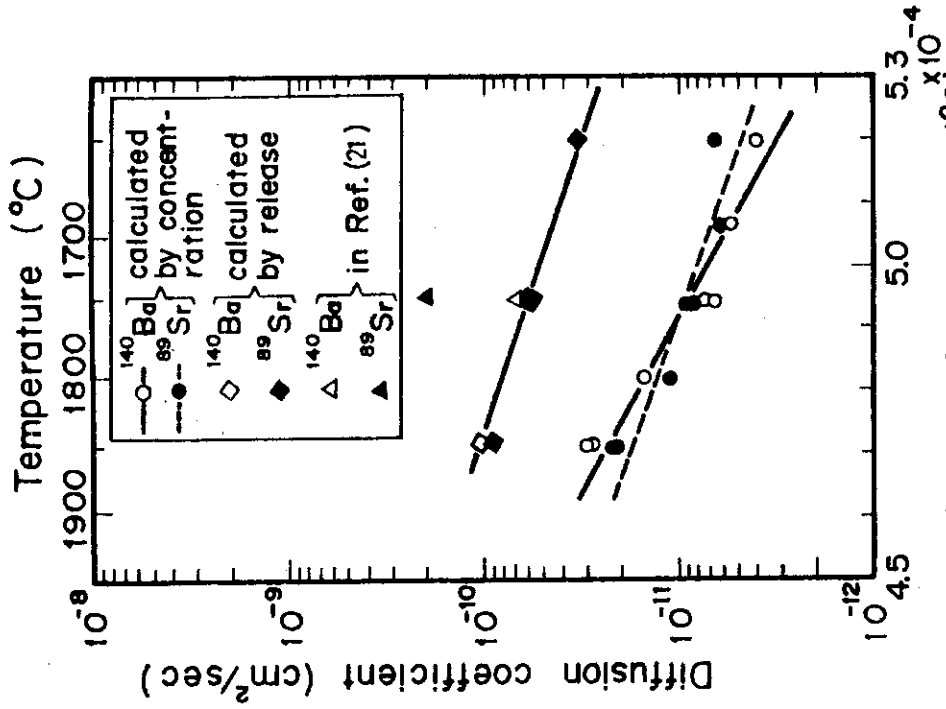

Fig. 27 Temperature dependences of ^{140}Ba and ^{89}Sr diffusion coefficients in the SiC layer.

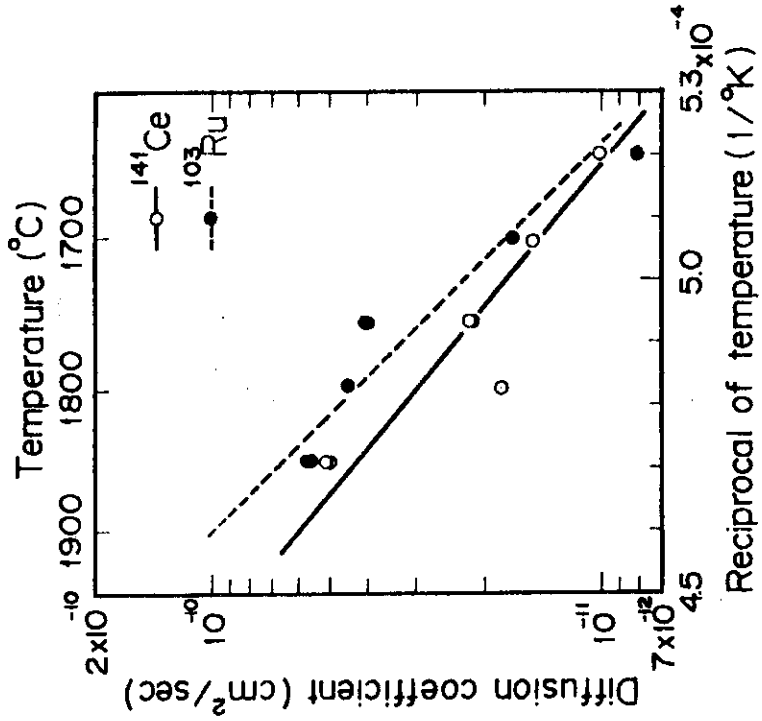

Fig. 28 Temperature dependences of ^{141}Ce and ^{103}Ru diffusion coefficients.

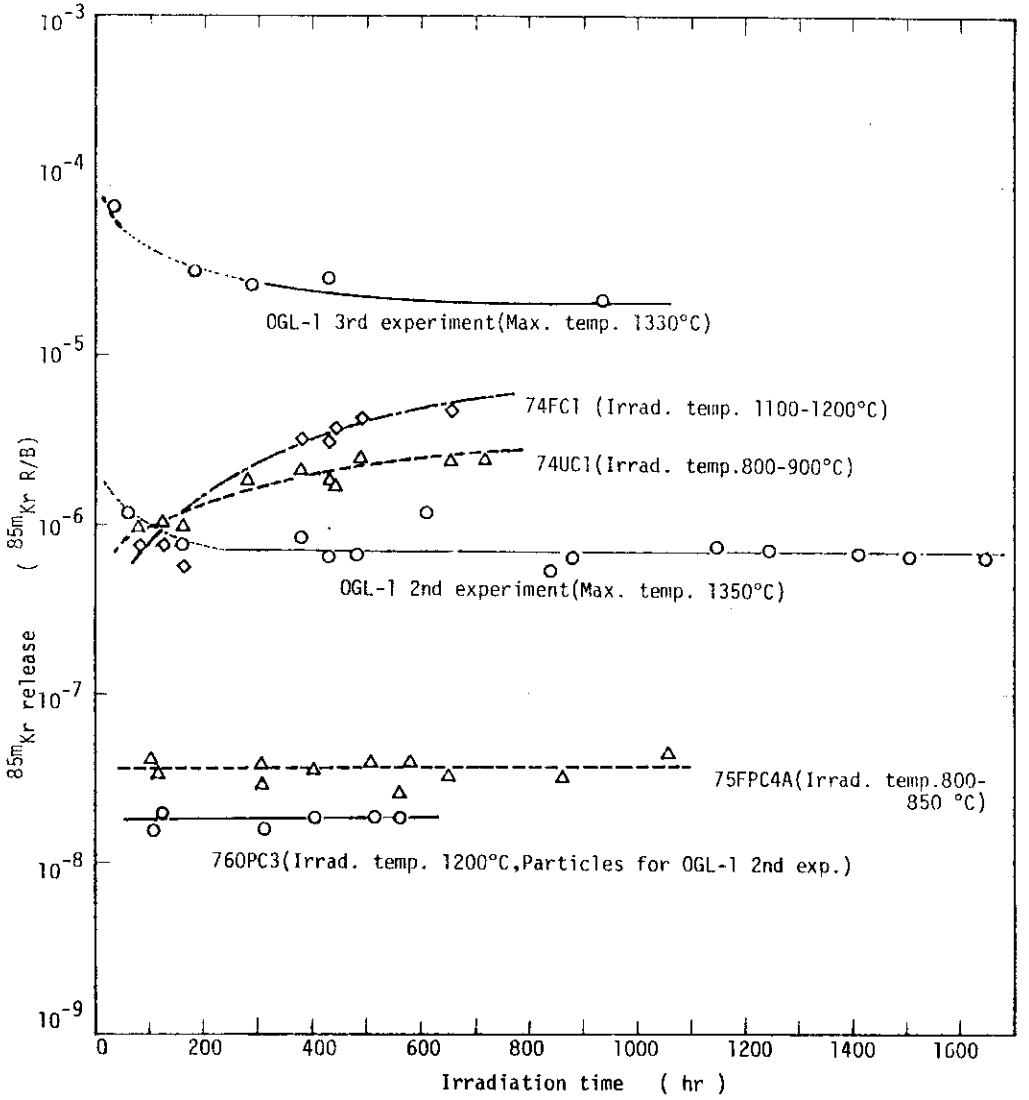

Fig. 29 Time dependence of FP gas release
(Gas swept capsules and OGL-1 experiments)

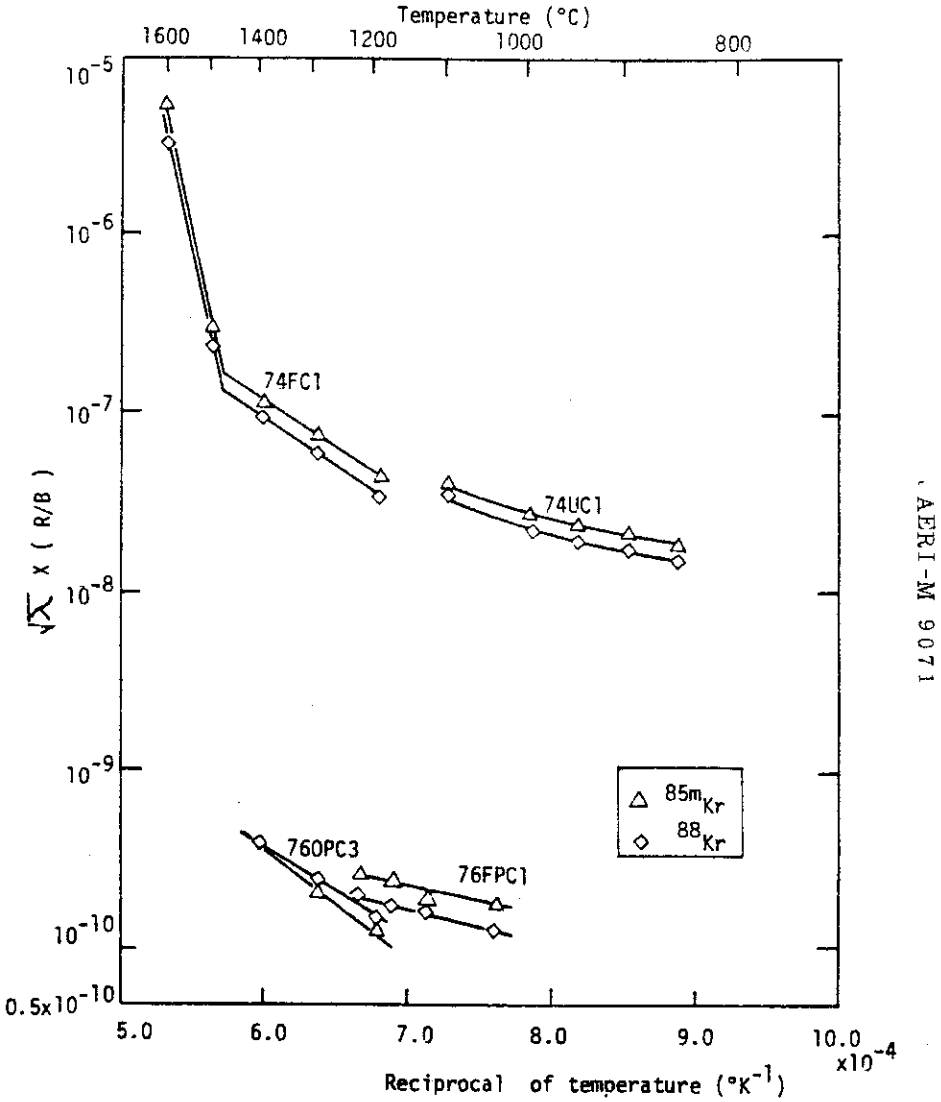

Fig. 30 Variation of $\sqrt{\chi}$(R/B) with reciprocal of temperature

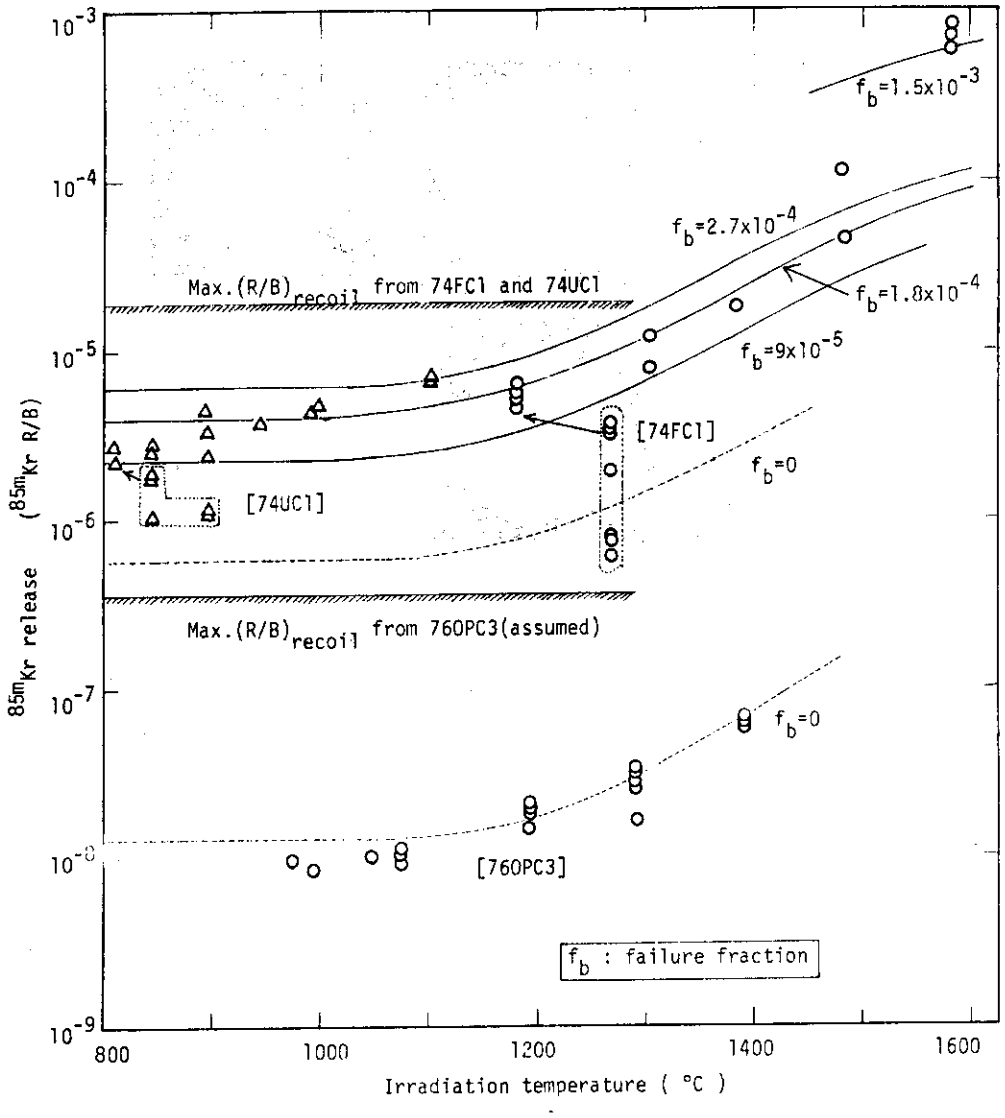

Fig. 31 Temperature dependence of FP gas release and estimation of the failure fraction of coated particles.

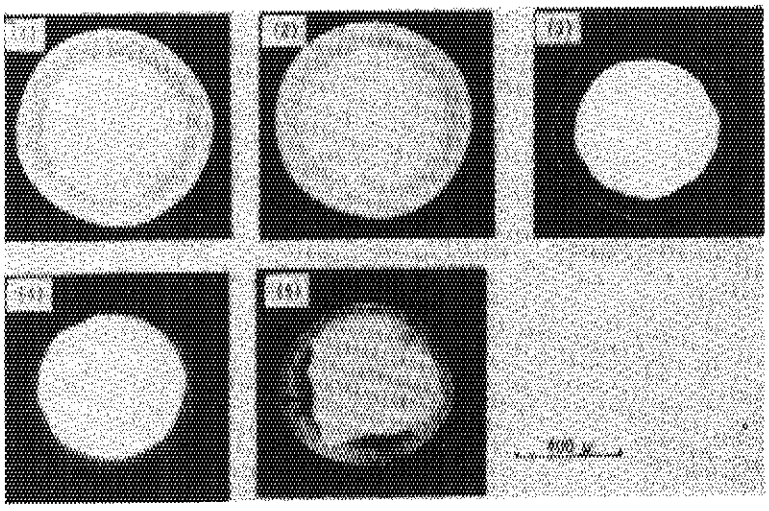

Fig. 32 Typical X-ray microradiographs showing the decrease of layer thickness; numbers in photos are identical to those in Fig. 33.

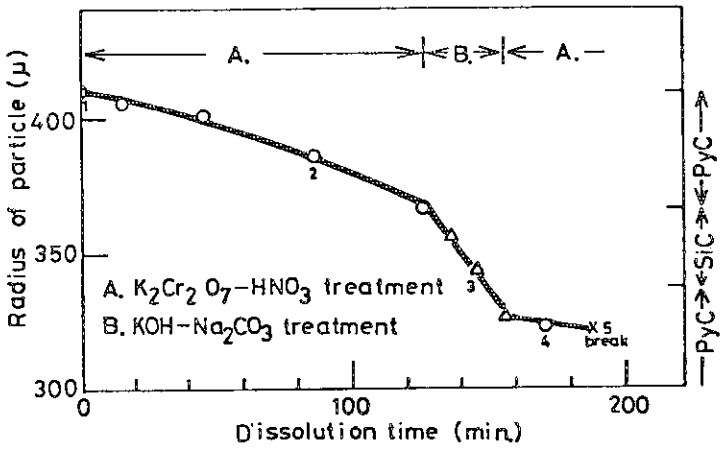

Fig. 33 Variation of coating layer thickness with dissolution steps.

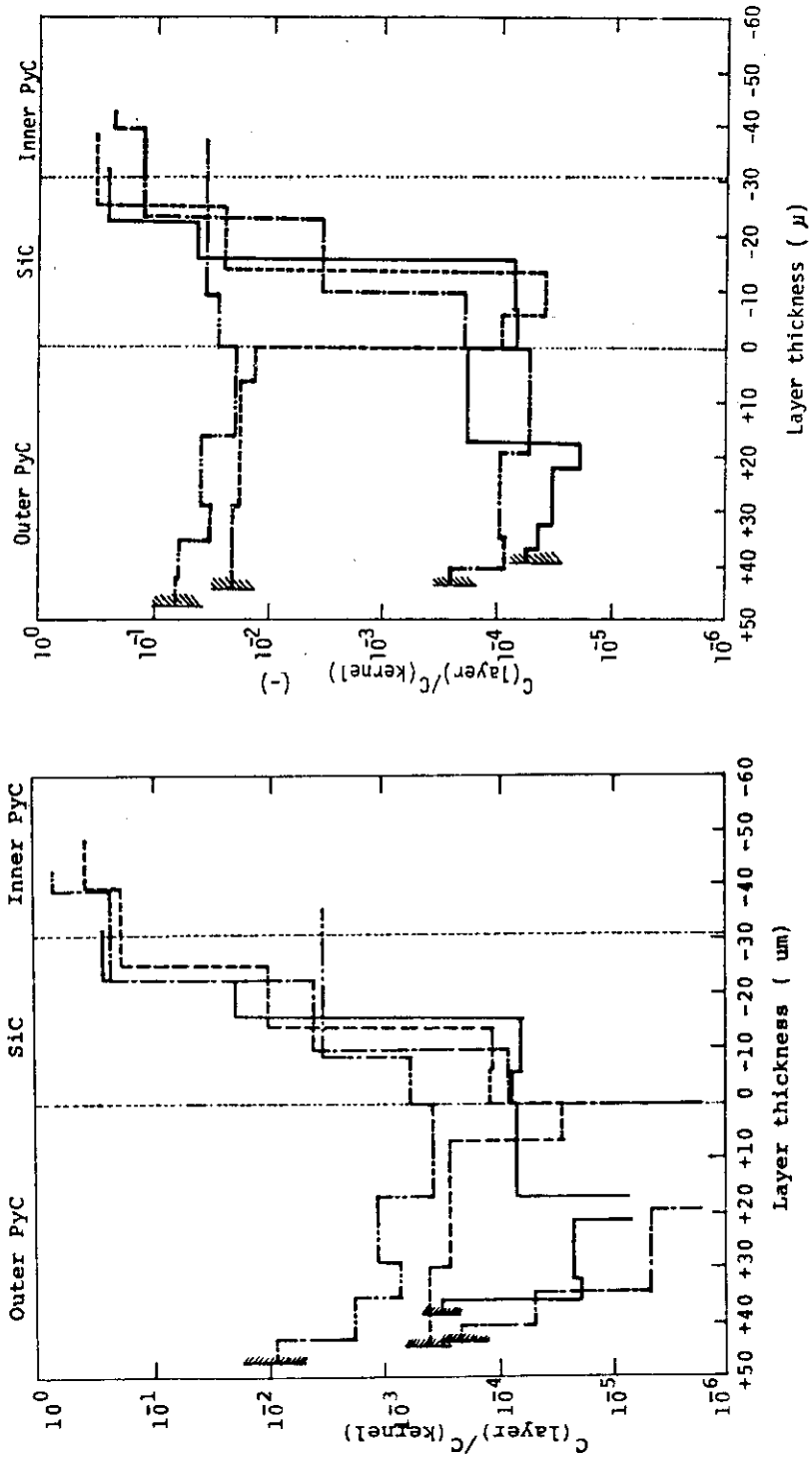

Fig. 34 Concentration distributions of ^{137}Cs(a) and ^{90}Sr(b) in the coating layers of the irradiated particles.

—·— Sample 1-A ------ Sample 1-C
—— Sample 1-B —··— Sample 2

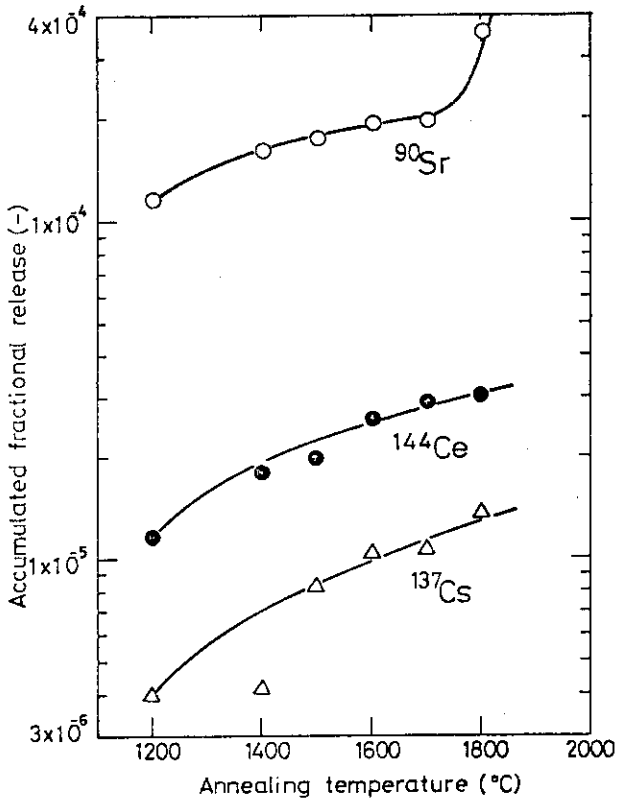

Fig. 35 Fractional releases of solid fission products from Sample 1-B in post irradiation heating.